Comparative study of water ice exposures on cometary nuclei using multispectral imaging data

Nilda Oklay, Jessica M. Sunshine, Maurizio Pajola, Antoine Pommerol, Jean-Baptiste Vincent, Stefano Mottola, Holger Sierks, Sonia Fornasier, M. Antonella Barucci, Frank Preusker, et al.

HAL Id: insu-01397742
https://insu.hal.science/insu-01397742

Submitted on 16 Jun 2017

Comparative study of water ice exposures on cometary nuclei using multispectral imaging data

N. Oklay,[1]⋆ J. M. Sunshine,[2] M. Pajola,[3,4] A. Pommerol,[5] J.-B. Vincent,[1]
S. Mottola,[6] H. Sierks,[1] S. Fornasier,[7] M. A. Barucci,[7] F. Preusker,[6] F. Scholten,[6]
L. M. Lara,[8] C. Barbieri,[9] P. L. Lamy,[10] R. Rodrigo,[11,12] D. Koschny,[13]
H. Rickman,[14,15] M. F. A'Hearn,[2] J.-L. Bertaux,[16] I. Bertini,[4] D. Bodewits,[2]
G. Cremonese,[17] V. Da Deppo,[18] B. J. R. Davidsson,[19] S. Debei,[20] M. De Cecco,[21]
J. Deller,[1] M. Fulle,[22] A. Gicquel,[1] O. Groussin,[23] P. J. Gutiérrez,[8] C. Güttler,[1] I. Hall,[1]
M. Hofmann,[1] S. F. Hviid,[6] W.-H. Ip,[24] L. Jorda,[23] H. U. Keller,[25] J. Knollenberg,[6]
G. Kovacs,[1] J.-R. Kramm,[1] E. Kührt,[6] M. Küppers,[26] M. Lazzarin,[9] Z.-Y. Lin,[24]
J. J. Lopez Moreno,[8] F. Marzari,[9] G. Naletto,[27,4,18] X. Shi,[1] N. Thomas[5]
and C. Tubiana[1]

Affiliations are listed at the end of the paper

ABSTRACT

Deep Impact, *EPOXI* and *Rosetta* missions visited comets 9P/Tempel 1, 103P/Hartley 2 and 67P/Churyumov-Gerasimenko, respectively. Each of these three missions was equipped with both multispectral imagers and infrared spectrometers. Bright blue features containing water ice were detected in each of these comet nuclei. We analysed multispectral properties of enriched water ice features observed via Optical, Spectroscopic, and Infrared Remote Imaging System narrow angle camera on comet 67P in the wavelength range of 260–1000 nm and then compared with multispectral data of water ice deposits observed on comets 9P and 103P. We characterize the UV/VIS properties of water-ice-rich features observed on the nuclei of these three comets. When compared to the average surface of each comet, our analysis shows that the water ice deposits seen on comet 9P are similar to the clustered water-ice-rich features seen on comet 67P, while the water ice deposit seen on comet 103P is more akin to two large isolated water-ice-rich features seen on comet 67P. Our results indicate that the water ice deposit observed on comet 103P contains more water ice than the water-ice-rich features observed on comets 9P and 67P, proportionally to the average surface of each nucleus.

Key words: methods: data analysis – techniques: image processing – techniques: imaging spectroscopy – comets: individual: 9P/Tempel 1 – comets: individual: 103P/Hartley 2 – comets: individual: 67P/Churyumov–Gerasimenko.

1 INTRODUCTION

Cometary missions *Deep Impact* (*DI*), *EPOXI* and *Rosetta* visited comets 9P (A'Hearn et al. 2005), 103P (A'Hearn et al. 2011) and 67P (Glassmeier et al. 2007; Taylor et al. 2015), respectively. The instrumentation of these three missions includes cameras equipped with filters allowing imaging at various wavelengths from near-

ultraviolet (NUV) to near-infrared (NIR). Moreover, each of these missions had infrared (IR) spectrometers to allow mineralogical studies of the observed comets and detection of water ice. Bright blue features were observed on the surfaces of each of these three comets (Sunshine et al. 2006, 2011; Li et al. 2013; Pommerol et al. 2015b; Oklay et al. 2016). Albedo of the water ice deposits detected on comet 9P is 1.8–2.2 times brighter than the average surface from IR to UV (Li et al. 2007). Some bright areas observed on comet 103P have more than twice the albedo of the average surface including a large bright area about three times the average

⋆ E-mail: oklay@mps.mpg.de

surface (Li et al. 2013). On comet 67P, there are bright features having reflectance of up to 10 times their surrounding (Pommerol et al. 2015b). The spectroscopic observations of those bright blue features in IR wavelengths unanimously identified the presence of water ice (Sunshine et al. 2006, 2011; Barucci et al. 2016; Filacchione et al. 2016c).

During *DI* and *EPOXI* flybys of comets 9P and 103P, respectively, spatial resolutions up to an order of 1 m px^{-1} were achieved. The nucleus of comet 67P is mapped in spatial resolutions up to 11 cm px^{-1} via narrow angle camera (NAC) of the Optical, Spectroscopic, and Infrared Remote Imaging System (OSIRIS; Keller et al. 2007). Using high spatial resolution multispectral images taken before 2015, three types of bright features were detected in the Northern hemisphere and the equatorial region of comet 67P (Pommerol et al. 2015b): clustered, isolated and boulders with bright patches. There were more than a hundred of bright features reported in the study of Pommerol et al. (2015b) and the analysis of those features from both multispectral data and spectroscopic data is an ongoing work. Water ice was found to be the most plausible explanation for the bright blue features[1] observed on comet 67P by Pommerol et al. (2015b) and this is confirmed on two of the large bright blue clusters by Filacchione et al. (2016c) and in eight of the bright spots by Barucci et al. (2016) via IR spectroscopic observations. Besides many other investigated surface features, the multispectral properties of one of the clusters where water ice was detected (Filacchione et al. 2016c, BAP2) were investigated by Oklay et al. (2016) together with the isolated water-ice-rich feature (Barucci et al. 2016, spot5) using OSIRIS NAC images and their multispectral similarities with the active regions observed on comet 67P were discussed. Moreover, the visual detection of jets rising from BAP2 of Filacchione et al. (2016c) was presented by Oklay et al. (2016) and Vincent et al. (2016). Via inversion techniques, the sources of some of the observed dust jets (Vincent et al. 2016) and outbursts (Knollenberg et al. 2016) were identified as water-ice-rich clusters and potentially water-ice-rich features. The multispectral analysis of the second cluster (Filacchione et al. 2016c, BAP1) where water ice was detected is included to this study.

The multispectral data of comets 9P, 103P and 67P display an increase in reflectance, i.e. red sloped from 260 to 1000 nm Li et al. (2007, 2013) and Sierks et al. (2015), respectively. Some spectral slope variations on smaller scales were observed on the surface of comet 67P when the nucleus was globally considered (Fornasier et al. 2015b). Once the active surface regions and water-ice-rich features of comet 67P were investigated in high spatial resolution images, multispectral analysis revealed the variety in spectral features and spectral slopes (Oklay et al. 2016). In the OSIRIS NAC spectral range, clustered bright features on comet 67P display bluer spectral slopes than the average surface, while isolated bright features have flat spectra (Pommerol et al. 2015b; Oklay et al. 2016). Water ice deposits observed on the surface of comets 9P and 103P also display bluer spectral slopes than their average surface spectra (Sunshine et al. 2006, 2011; Li et al. 2013). Both clustered and isolated bright features have high signals in the NUV wavelengths, which make them appear blue in colour composites generated by using the images taken in NIR, visible and NUV wavelengths (Pommerol et al. 2015b; Oklay et al. 2016). This

is also valid for the water ice deposits observed on comets 9P and 103P (Sunshine et al. 2006, 2011; Li et al. 2013).

Physical properties of the detected water-ice-rich features were derived from the IR observations for comets 9P, 103P and 67P (Sunshine et al. 2006, 2011; Li et al. 2013; Filacchione et al. 2016c). The water ice absorption bands at 1.5, 2.0 and 3.0 μm are common in the IR spectra of these three comets. Water ice deposits observed on comet 9P were modelled by areal mixing of 30 μm-sized water ice particles (6 per cent) with dark material (Sunshine et al. 2006), while water-ice-rich clusters on comet 67P were explained by areal mixing of 2 mm-sized pure water ice (1.2 per cent) with dark material and intimate mixture of 56 μm-sized water ice particles (3.4 per cent) with dark material (Filacchione et al. 2016c). The modelling of IR spectra shows that the water-ice-rich features observed on these comets contain very small amount of water ice (<6 per cent).

Due to its high albedo and low spectral slope values, the Hapi region of comet 67P was concluded to have higher water abundance by Fornasier et al. (2015b). Analysis of IR spectra of Hapi revealed the existence of a diurnal cycle of water ice near a shadowed region on Hapi (De Sanctis et al. 2015). Moreover, water frost is observed all over the comet 67P at the local morning following the shadow line and retreating with shadows and disappearing with the increase of illumination (Fornasier et al. 2015a). This very small-scale frost is a transient event, which makes it out of the focus of our comparative work.

Spectral analysis of Oklay et al. (2016) identified two types of active regions:

(i) isolated bright blue features observed in Imhotep, where in one water ice is detected,

(ii) Hapi, active pits, alcoves and clustered bright blue features where water ice is detected.

Such colour variations are possibly associated with different ice formation mechanisms discussed by De Sanctis et al. (2015) and Filacchione et al. (2016c): micrometre-sized water ice grains as a result of fast condensation of water vapour, millimetre-sized pure water ice grains observed over a 100 m-sized regions as a result of exposure of deeper layers. Filacchione et al. (2016c) concluded two formation mechanisms to explain water ice exposed from beneath the surface: by grain growth due to vapour diffusion in water-ice-rich subsurface layers or by water ice grain sintering.

The Southern hemisphere of comet 67P started to be illuminated on spring 2015 and two large water-ice-rich patches were reported by Fornasier et al. (2016) in Anhur region (see El-Maarry et al. 2016, for region definitions). These two patches are located in smooth regions unlike the water-ice-rich features observed on the Northern hemisphere of the comet, which are mostly seen in taluses and located below cliffs and overhangs. The water-ice-rich features observed on the Northern hemisphere are long lived (half a year for clusters and more than 1.5 yr for isolated ones Section 3.4), while the two enriched water ice patches observed on the Southern hemisphere survived only for about 10 d (Fornasier et al. 2016). Those patches observed in Anhur region were found to contain also CO_2 ice, which disappeared on a time-scale of days (Filacchione et al. 2016a,b). Analysis of the enriched water ice patches observed in the Southern hemisphere of comet 67P is an ongoing work and will not be discussed further in this study.

This work focuses on the comparison of the water-ice-rich features observed on the surface of comets 9P, 103P and 67P using multispectral imaging data. For this comparison, we analysed bright blue features where water ice was previously detected via IR observations (Filacchione et al. 2016c; Barucci et al. 2016). Here, we

---

[1] In this study, the bright blue features where water ice was detected by IR observations are called water ice features, while all other bright features concluded to contain water ice by OSIRIS observations are called potentially water ice features.

Table 1. Multispectral images used in this study. Image IDs are in the format of comet name, instrument name, image set number. Additional image set of Hapi region of comet 67P is also included.

Image ID	Acquisition date	UT	Central wavelength (nm)	r (au)	Resolution (m px^{-1})	Phase angle (°)
67P-NAC#1	2014-09-05	05:31:25	360.0, 535.7, 649.2, **701.2**, 743.7, 882.1, 989.3	3.43	0.76	57.31
67P-NAC#2	2014-09-05	06:36:14	360.0, 535.7, 649.2, **701.2**, 743.7, 882.1, 989.3	3.43	0.76	57.76
67P-NAC#3	2014-09-05	06:46:25	360.0, 535.7, 649.2, **701.2**, 743.7, 882.1, 989.3	3.43	0.76	57.85
67P-NAC-Hapi	2014-08-22	01:41:55	360.0, 480.7, 535.7, **649.2**, 701.2, 743.7, 805.3, 882.1, 989.3	3.51	1.21	34.84
9P-HRI#1	2005-07-04	05:44:36	350.0, 450.0, 550.0, 650.0, 750.0, 850.0, 950.0	1.51	16	62.9
103P-HRI#1	2010-11-04	13:49:44	350.0, 450.0, 550.0, 650.0, 750.0, 850.0, 950.0	1.06	14	85.3
9P-MRI#1	2005-07-04	05:44:36	309.0, 345.0, 387.0, 514.0, 526.0, 750.0, 950.0	1.51	82	62.9

Notes. Acquisition time (UT) is given for the reference image. Reference images are indicated in bold. Image IDs are used as a reference in all images displayed in this work. All data are in reflectance (radiance factor).

Table 2. Multispectral NAC images used for the temporal evolution analysis of the enriched water ice features.

Image ID	Acquisition date	UT	Central wavelength (nm)	r (au)	Resolution (m px^{-1})	Phase angle (°)
67P-NAC#T1	2014-09-05	06:36:14	360.0, 535.7, 649.2, **701.2**, 743.7, 882.1, 989.3	3.43	0.76	57.76
67P-NAC#T2	2014-09-05	06:46:25	360.0, 535.7, 649.2, **701.2**, 743.7, 882.1, 989.3	3.43	0.76	57.85
67P-NAC#T3	2016-01-24	01:06:56	480.7, **649.2**, 882.1	2.04	1.37	61.08

Notes. Acquisition time (UT) is given for the reference image. Reference images are indicated in bold. Image IDs are used as a reference in all images displayed in this work.

note that these features are not pure water ice features but enriched in water ice. Moreover, association of bright blue features with water ice is well known and presented for each of these three comets in earlier studies (see main text). Due to long-term observations of comet 67P, the investigation of bright blue features detected by OSIRIS in the IR wavelengths is an ongoing work. Therefore, the existence of water ice is not yet confirmed in all bright blue features observed on comet 67P. However our analysis includes several bright blue features (see Fig. B1) which show almost identical multispectral properties to those where water ice was detected. These additional features are therefore considered as likely water-ice-rich features.

We study the multispectral properties of water ice features observed in the Northern hemisphere of comet 67P before 2015, and compare them to those of Sunshine et al. (2006, 2011) for comets 9P and 103P using various spectral analysis techniques (Section 2.1), as well as statistical methods (Section 2.3). For further investigation of the water ice features, laboratory data of water ice mixtures described in Section 2.4 are studied.

2 IMAGING DATA AND ANALYSIS METHODS

The scientific cameras High Resolution Imager (*DI*-HRI; Hampton et al. 2005) and OSIRIS NAC (Keller et al. 2007) are equipped with filters centred at similar wavelengths and have similar transmissions. Common wavelength range of both instruments is 300–1050 nm. Medium Resolution Imager (*DI*-MRI; Hampton et al. 2005) is also equipped with filters which are mainly narrow band. With these three instruments, imaging in different filters is not done simultaneously but subsequently. During such multispectral imaging, the observed surface has a motion due to the combined effects of comet rotation and spacecraft's orbital motion. Therefore, images taken at different wavelengths should be co-aligned and photometrically corrected before performing multispectral analysis. Sections 2.1

and 2.2 describe how image registration and photometric correction is achieved on OSIRIS NAC, *DI*-HRI and *DI*-MRI images. All images used in this study are *I/F* (radiance factor):

$$I/F = \frac{\pi r^2 I_{\mathrm{m}}}{F_{\odot}}, \qquad (1)$$

where I_{m} is the measured intensity in radiance units (Wm^{-2} nm^{-1} sr^{-1}, at the central wavelengths of each filter), $F_{\odot}$ is solar flux at 1 au measured at the central wavelength for each filter and r is the heliocentric distance of the comet in astronomical units.

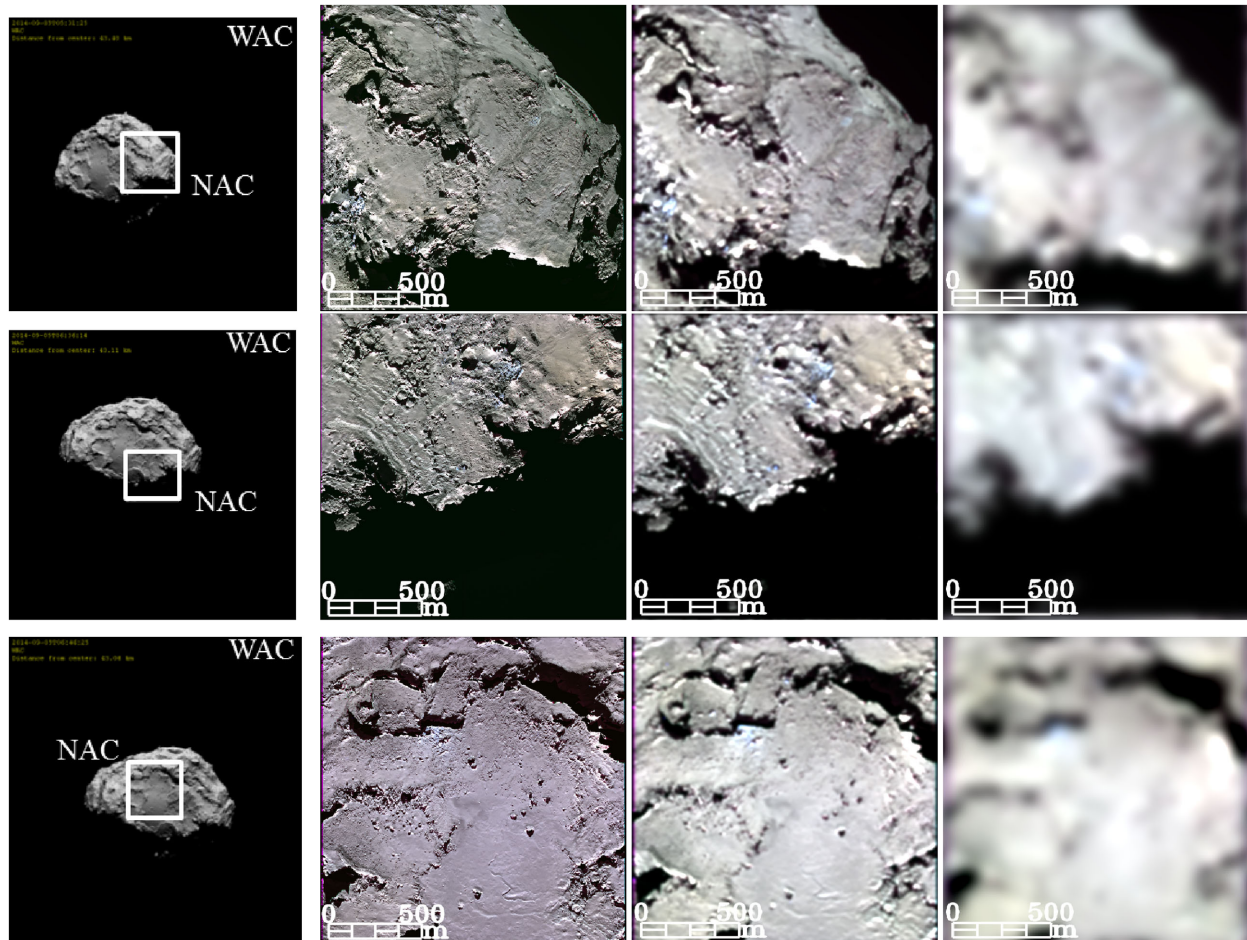## 2.1 OSIRIS NAC multispectral cubes

OSIRIS NAC images given in Tables 1 and 2 are co-aligned to eliminate colour artefacts created by misalignment of the images and photometrically corrected using Lommel–Seeliger disc law (Hapke 1993) to eliminate the effects due to different illumination conditions using Integrated Software for Imagers and Spectrometers (USGS ISIS3;[2] Anderson et al. 2004) software. Lommel–Seeliger disc definition included in the ISIS3 software is

$$D(\mathrm{i, e}) = \frac{2\cos(\mathrm{i})}{\cos(\mathrm{i}) + \cos(\mathrm{e})}, \qquad (2)$$

where D is the disc function with geometric angles incidence (i) and emission (e). Disc-corrected images are then obtained by dividing the *I/F* images by the disc function. In the photometrically corrected images, the regions with angles larger than 80° are excluded. The photometric angles are calculated from the 3D shape model described in Preusker et al. (2015), reduced to one million facets (sampling distance of about 8 m) to limit the necessary computational time. The SPICE kernels[3] are used with SPICE

[2] http://isis.astrogeology.usgs.gov/index.html
[3] http://www.cosmos.esa.int/web/spice/spice-for-rosetta

Figure 1. Colour composites of comet 67P at various spatial resolutions. Images taken at 989.9, 649.2 and 360.0 nm are assigned to the RGB channels of the images, respectively. The left-hand column shows the simulated views of the observations from the OSIRIS wide angle camera field of view, with NAC views marked in white rectangles. Image sets from #1 to #3 (Table 1) are given from top to bottom panels, respectively. Second column from the left shows the image sets in original NAC resolution (76 cm px^{-1}), second column from the right shows the image sets at *DI*-HRI spatial resolution (16 m px^{-1}, during comet 9P observations) and the right-hand column shows the image sets at *DI*-MRI spatial resolution (82 m px^{-1}, during comet 9P observations). Image stretches are unique for each image to emphasize the blue patches better within each set. Blue colours indicate water-ice-rich and potentially water-ice-rich features on the surface of comet 67P. The locations of the blue features are marked in Fig. B1 for each data set with zoom-ins in extra panels.

toolkit for c^4 for the alignment of the shape at the observing time of the reference images. Each step for the production of photometrically corrected multispectral data from subsequently taken OSIRIS NAC images are described in Oklay et al. (2016, appendix A).
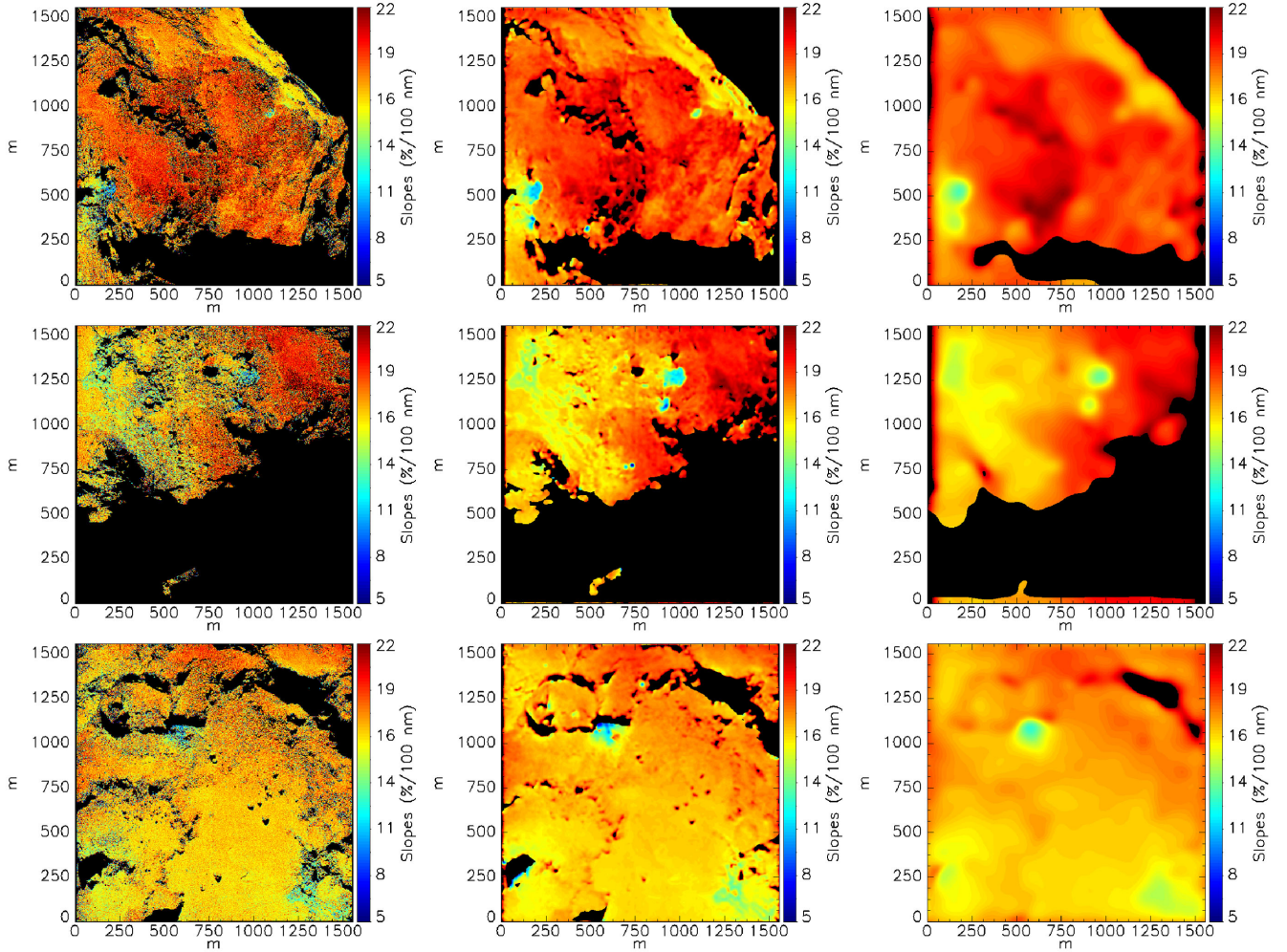
The bright blue (water-ice-rich) features observed on comet 67P are investigated using photometrically corrected and registered multispectral NAC data in small regions, where there is water ice. The borders of the investigated features are defined by using regions of interest (ROI) tools of ENVI version 5.0 (Exelis Visual Information Solutions, Boulder, Colorado) software and with self-written IDL (version 8.2) procedures.

Each NAC colour set given in Tables 1 and 2 contains clustered and isolated bright features including not only the features concluded to contain water ice as a result of detailed multispectral analysis (Pommerol et al. 2015b; Oklay et al. 2016) but also the features confirmed to contain water ice by the IR observations (Barucci et al. 2016; Filacchione et al. 2016c). All these features are introduced in Fig. B1 per image sets given in Table 1. The locations

of these features are marked on the map of comet 67P (Fig. A1) to show their distribution on the surface. Their sizes, coordinates and references for water ice prediction/confirmation are given in Table A1. The image sets given in Table 2 are used for the temporal analysis of the bright features, while the image sets given in Table 1 are used for the comparison of water-ice-rich features on all three comet nuclei.

In order to perform a comparison between the images taken in various spatial resolutions, all NAC data colour sets are convolved with two different 2D rotationally symmetric Gaussian functions, one having full width at half-maximum of the deconvolved *DI*-HRI spatial resolution (16 m px^{-1}) and the other one having *DI*-MRI spatial resolution (82 m px^{-1}). The data sets given in Table 1 are displayed in various resolutions in Fig. 1. Images taken with filters centred at wavelengths 989.3, 649.2 and 360.0 nm are used to generate the red, green, blue (RGB) images displayed in Fig. 1. Such colour composites are reliable tools to detect water-ice-rich features on the surface of comet 67P, with blue colour indicating the presence of volatiles (Oklay et al. 2016). Under the right observing conditions, those blue regions indicate active regions as well (Oklay et al. 2016; Vincent et al. 2016).

Figure 2. Spectral slopes of the investigated NAC images in various spatial resolutions. Spectral slopes displayed in the left-hand column are in original NAC resolution (76 cm px^{-1}), the ones displayed in the middle column are in *DI*-HRI spatial resolution (16 m px^{-1} during comet 9P observations) and the ones displayed in the right-hand column are in *DI*-MRI spatial resolution (82 m px^{-1} during comet 9P observations). Data sets (Table 1) from #1 to #3 are displayed from top to bottom. Corresponding phase angles are 57°31, 57°76 and 57°85, respectively. Spectral slopes lower than 13 per cent/100 nm indicate active surface, while values 13–15 per cent/100 nm indicate regions either peppered with small active regions or regions covered with airfall material. The inactive surface has spectral slope values above 15 per cent/100 nm. Water-ice-rich and potentially water-ice-rich features have spectral slope values lower than 13 per cent/100 nm.

Spectral slopes (Fig. 2) represent a good diagnostic to detect various surface units (Fornasier et al. 2015b; Oklay et al. 2016) and investigate variegation on the surface regions of comet 67P (La Forgia et al. 2015; Lucchetti et al. 2016; Pajola et al. 2016b). Therefore, this method is adopted to investigate the images given in Table. 1. Spectral slopes used in this study are defined as

$$\text{Spectral slope [per cent/100 nm]} = \frac{(R_{882.1} - R_{535.7}) x\, 10\,000}{(882.1 - 535.7) x (R_{535.7})}, \tag{3}$$

where R are the radiance factors in the given filters with their central wavelengths located at 882.1 and 535.7 nm.
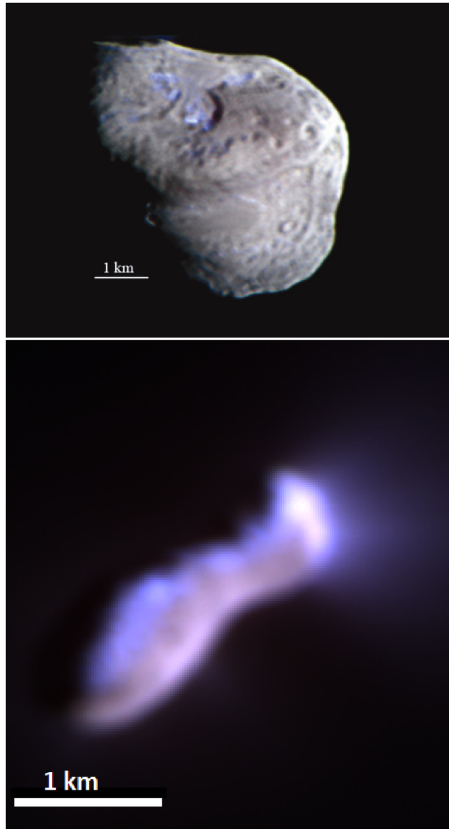
2.2 *DI*-HRI and *DI*-MRI multispectral cubes

The multispectral data of comets 9P and 103P given in Table 1 are displayed in Fig. 3 as colour composites. These colour composites are generated by using deconvolved images described in Lindler et al. (2007). In order to enhance the blue water ice regions, blue channels of both images are stretched. The images taken in NIR, visible and NUV wavelengths (see caption of Fig. 3 for exact wavelengths used per image composite) are used in the RGB channels of the images, respectively. All images of comets 9P and 103P are radiance factor. The multispectral data of comet 9P used in this study are described in Sunshine et al. (2006), while the data of comet 103P are described in Li et al. (2013). The calibration of the data obtained during flybys of comets 9P and 103P is given in Klaasen et al. (2008) and Klaasen et al. (2013), respectively.

2.3 Size distribution of bright features within the observed patches

The data set of images we used to identify the bright boulder is presented in Table 1. All the images are characterized by a scale of 0.76 m px^{-1}. This gave the possibility to derive a meaningful statistics of boulders with a diameter ≥2.1 m, i.e. the 3 pixels sampling which minimizes the likelihood of misidentifications of what we are detecting (Nyquist 1928). Moreover, since the observations

Figure 3. Colour composites of comets 9P (top panel) and 103P (bottom panel). Images taken in 950, 750 and 450 nm are used in the RGB channels of the top image, while images taken in 950, 750 and 345 nm are used in the RGB channels of the bottom image. Water ice deposits are seen in blue.

were performed with a phase angle of 57°, the presence of elongated shadows on the surface helped us in identifying even smaller boulders of the order of 2 pixels in diameter, i.e. 1.4–1.8 m. None the less, as previously presented in Pajola et al. (2015) and Pajola et al. (2016a), we decided not to include these populations in the cumulative size–frequency distribution because they are not a complete data set. Indeed, as plots in Fig. 8 show, below the 2.1 m value limit, the cumulative number of boulders starts to roll over, indicating that the data set at these sizes may not be complete. Boulders are defined as positive reliefs which are detectable in multiple images obtained with different geometries, with the constant presence of an elongated shadow. We manually identified them and measured their position on the comet's surface by using the ARCGIS software. We therefore assumed their shapes as circumcircles, deriving their diameter and the corresponding area. We consequently derived the cumulative size–frequency distribution, and by fitting a regression line to the logarithmic data, we obtained the power-slope indices presented in all plots.[5]

2.4 Analysis of the laboratory data

Laboratory experiments of water ice mixtures performed by Pommerol et al. (2015a) were used to study water ice exposures

observed on the surface of comet 67P (Pommerol et al. 2015b) and to investigate active regions together with some bright blue features (Oklay et al. 2016) observed on comet 67P. The spectral similarities of those laboratory data to the spectra of observed features help on the conclusion of the water ice exposures on the surface of comet 67P.

Poch et al. (2016) performed further laboratory experiments on the sublimation of intra- and intermixtures of water ice with minerals and organic matter. Textural, compositional and spectral properties of those mixtures were described and discussed with implications for comets (Poch et al. 2016). Besides the high reflectance of the laboratory spectra, the spectral shapes of water ice mixtures are comparable to the spectral properties of water-ice-rich features seen on comet 67P in the visible wavelength range (Pommerol et al. 2015b; Oklay et al. 2016). Therefore, the laboratory data given in Pommerol et al. (2015a) and Poch et al. (2016) are resampled using the NAC filter transmissions following the data reduction process described in Oklay et al. (2015). Resampled laboratory data are then investigated in relative reflectance[6] for the comparison of the water-ice-rich features observed on comet 67P with the laboratory data.
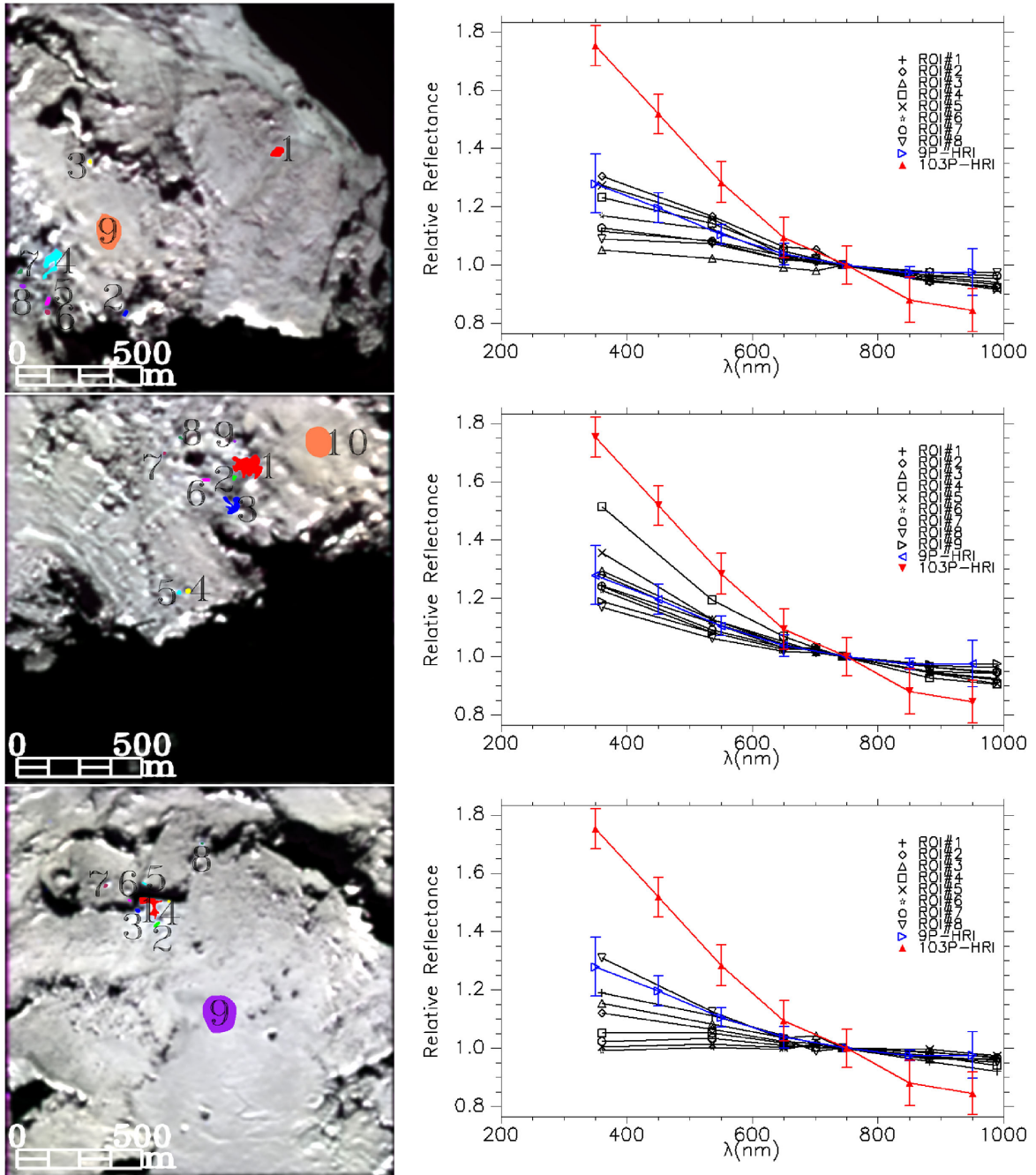
3 RESULTS

In the analysis of the water ice exposures observed on comets 9P, 103P and 67P, we used the multispectral data given in Table 1. The water ice and potentially water ice features seen in the OSIRIS NAC images (Fig. B1) are investigated in ROI. Resistant mean spectra (hereafter mean spectra) excluding data points deviating by more than $\pm 3\sigma$ of the median per investigated ROI are then calculated for further analysis. For a direct comparison, the mean spectra of the selected ROIs are normalized at 750 nm to remove the first-order effects of photometry, which due to limitations in resolution and thus topographic knowledge is not well known for all comets at the scale of the water icy deposits.

In order to compare the results taken at different phase angles, from different regions, from different comets and with different instruments, we focus our multispectral analysis on relative colour. We normalize the data to the local comet background to remove any minor spectral differences between surfaces. This is particularly important as blue water icy components are expected to be of the order of <6 per cent (Sunshine et al. 2006; Barucci et al. 2016; Filacchione et al. 2016c) and thus the absolute (reflectance) data would be dominated by the spectral properties of the bare nuclei. Here, we note that water ice signals are in sub-pixel scales, thus a significant component of any signal measured is non-ice, which varies from comet to comet. Normalizing by nearby pixels allows us to better compare the ice components between comets and provides a first-order correction for difference in phase reddening. For comet 103P and to a lesser extent comet 9P phase correction cannot be explicitly made, as the shape model is not known well enough to determine the local incidence and emission angles at the scales of water icy deposits. Using the relative multispectral data, we best compare and interpret observations from different comets under different illumination conditions and acquired with different instruments. When comparing multispectral data of comet 67P with laboratory data, normalized reflectance at 535.7 nm is used (see Section 3.5).

---

[5] The vertical error bars indicate the root of the cumulative number of counting boulders, as in Pommerol et al. (2015b).

[6] Reflectance normalized at 535.7 nm.

Figure 4. Selected ROIs on the NAC image sets (from top to bottom) in *DI*-HRI spatial resolution (left-hand panel) with relative reflectance calculated in each ROI (right-hand panel) together with the spectra of water ice deposits observed on comets 9P and 103P. Typical standard deviations of the data points from the resistant mean are 8.93×10^{-5}, 9.64×10^{-5}, 1.44×10^{-4} from top to bottom. The ROIs with largest # represent the average surface, where the mean spectra of each ROI are normalized (see Fig. B3 for the spectra).
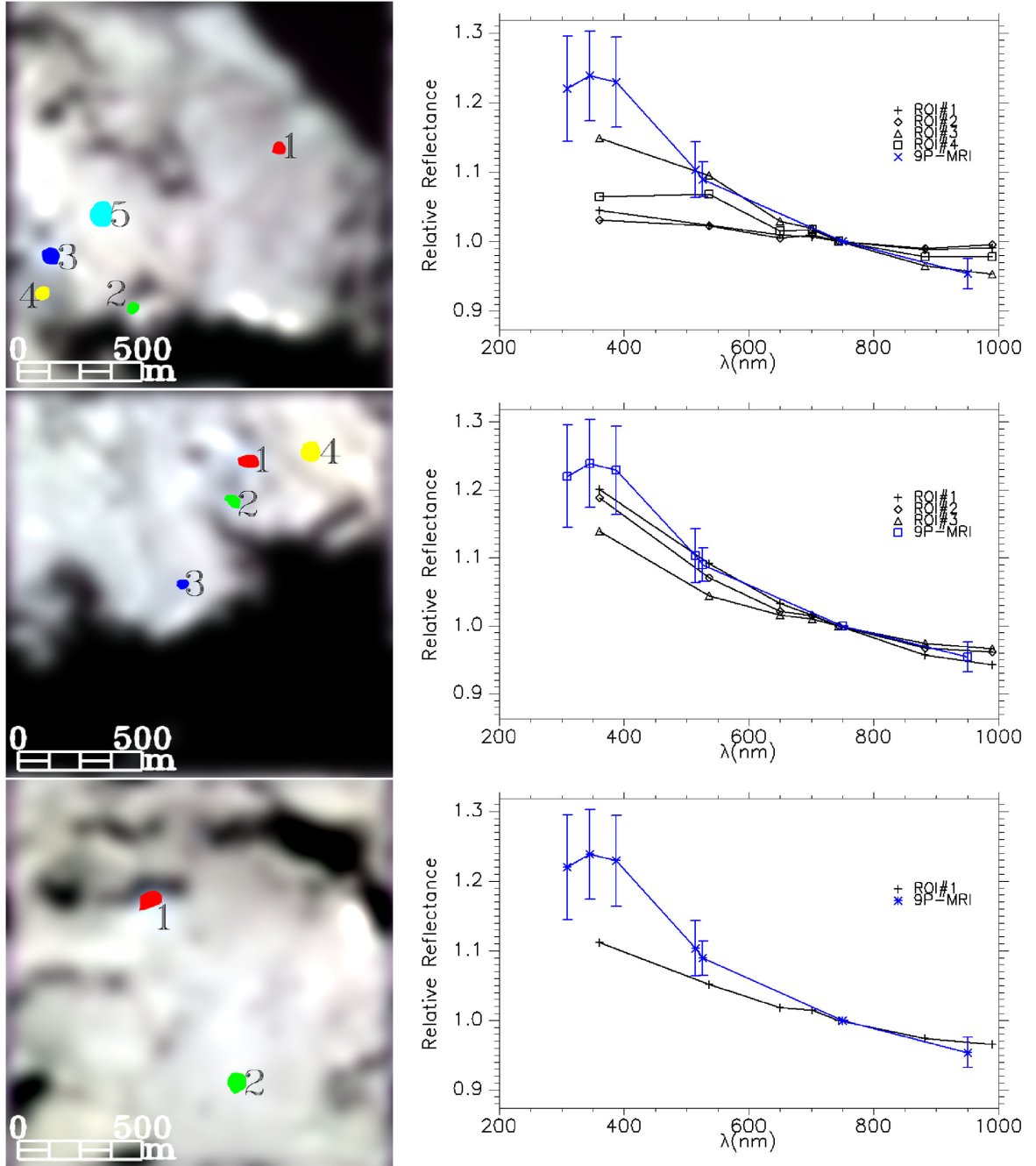
The water ice deposits observed on comets 9P and 103P are shown as blue patches in Fig. B2, while the average surface used in the normalization per image set is indicated in red rectangles. The mean spectra of these water ice deposits are presented with the average surface spectra in Fig. B4[7] to present the spectral differences of the

features with respect to the average surface. ROIs defined on comet 67P images are presented in the left-hand columns of Figs 4, 5 and 7. The ROI with the largest # in each data set represents the average surface. All mean surface spectra used in this study are presented in Fig. B3.

We compared relative reflectance of each ROI selected on the images of comet 67P with the relative reflectance of water ice deposits observed on comets 9P and 103P to detect similarities/dissimilarities of the investigated features.

---

[7] The same is presented in the right-hand panels of Fig. 11 for the comet 67P data.

Figure 5. Selected ROIs on the NAC image sets (from top to bottom) in *DI*-MRI spatial resolution (left-hand panel) with relative reflectance calculated in each ROI (right-hand panel) together with the spectra of water ice deposits observed on comets 9P and 103P. Typical standard deviations of the data points from the resistant mean are 8.93×10^{-6}, 5.15×10^{-6}, 1.55×10^{-5} from top to bottom. The ROIs with largest # represent the average surface, where the mean spectra of each ROI are normalized (see Fig. B3 for the spectra).

3.1 Comparison using multispectral imaging data

Co-aligned and photometrically corrected multispectral data sets of comet 67P given in Table 1 are presented as RGB colour composites generated by using the images taken at 882.1, 649.2 and 360.0 nm wavelengths. The simulated wide angle camera views of the NAC observations are shown in the left-hand column of Fig. 1 per data set (from top to bottom) as context. The corresponding NAC images are shown in the second column of Fig. 1, while the same images in *DI*-HRI (16 m px^{-1}) and *DI*-MRI (82 m px^{-1}) spatial

resolutions are given in the third and fourth columns. The observed region (Imhotep and its vicinity, hereafter extended Imhotep) of comet 67P is grey in this colour scheme, while the water-ice-rich and potentially water-ice-rich features are blue. Potentially active surrounding of roundish features observed in this region is green. These roundish features will be discussed in Section 3.4 further. The water-ice-rich features BAP1, 2 (Filacchione et al. 2016c) and spots 5 and 7 (Barucci et al. 2016) are detectable at each spatial resolution investigated in this study (see Fig. B1 for the individual features in

high spatial resolution). The images in the last two panels of Fig. 1 are considered for the comparative study presented in this section and in Section 3.2.

Two types of water ice and potentially water ice features are seen in the image sets displayed in Fig. B1. The first type is represented by clusters having about 150 m long blue debris fields extending from their neighbouring cliffs or overhangs. In those features, the neighbouring cliff (or overhang) has blue edges (see Fig. B1) indicating a cliff collapse and exposure of water ice from below the surface. The formation of those clusters is discussed in Section 3.3 in more details. Due to their large areas, these clusters are detectable in RGB colour composites even at resolutions down to 82 m px^{-1}. The second type is represented by isolated features, mainly located below overhangs. These isolated features are usually small, limited to the spatial resolution of the observations. Such small features would not be detectable at the spatial resolutions achieved during comet 9P and 103P observations. However, there are some large isolated bright features about 10 m scales (Fig. 9) which are detectable in lower spatial resolutions (see last two columns of Fig. 1).

Spectral slopes given in Fig. 2 allow quantitative comparison of the water-ice-rich and potentially water-ice-rich features in various spatial resolutions. Since these image sets were taken subsequently, the phase angle varies only 0°.5. Therefore, the phase reddening given in Fornasier et al. (2015b) is negligible. The overall observed region (extended Imhotep) has spectral slopes above 15 per cent/100 nm with local low spectral sloped sub-regions. The water-ice-rich and potentially water-ice-rich features have spectral slope values between 8 and 13 per cent/100 nm, which makes them part of the active group defined by Oklay et al. (2016). Indeed in one, jets were detected. The lack of activity feature detection in the other investigated features must be due to limited observing conditions, which were not allowing the detection of such small-scale events. The surroundings of roundish features seen in images sets #2 and #3 have also lower spectral slope values than the average surface which are only 1–2 per cent/100 nm higher than the water-ice-rich features. Due to their spectral properties, they were classified within the active group by Oklay et al. (2016) and the source region of outburst seen on 2015-03-12 is one of these roundish feature (Knollenberg et al. 2016). Even though the spectral properties of those features are very similar to the clusters where water ice was detected (Oklay et al. 2016, fig. 9b), there was no water ice detection on them. Therefore, they are not included to our comparative study but discussed in Section 3.4.
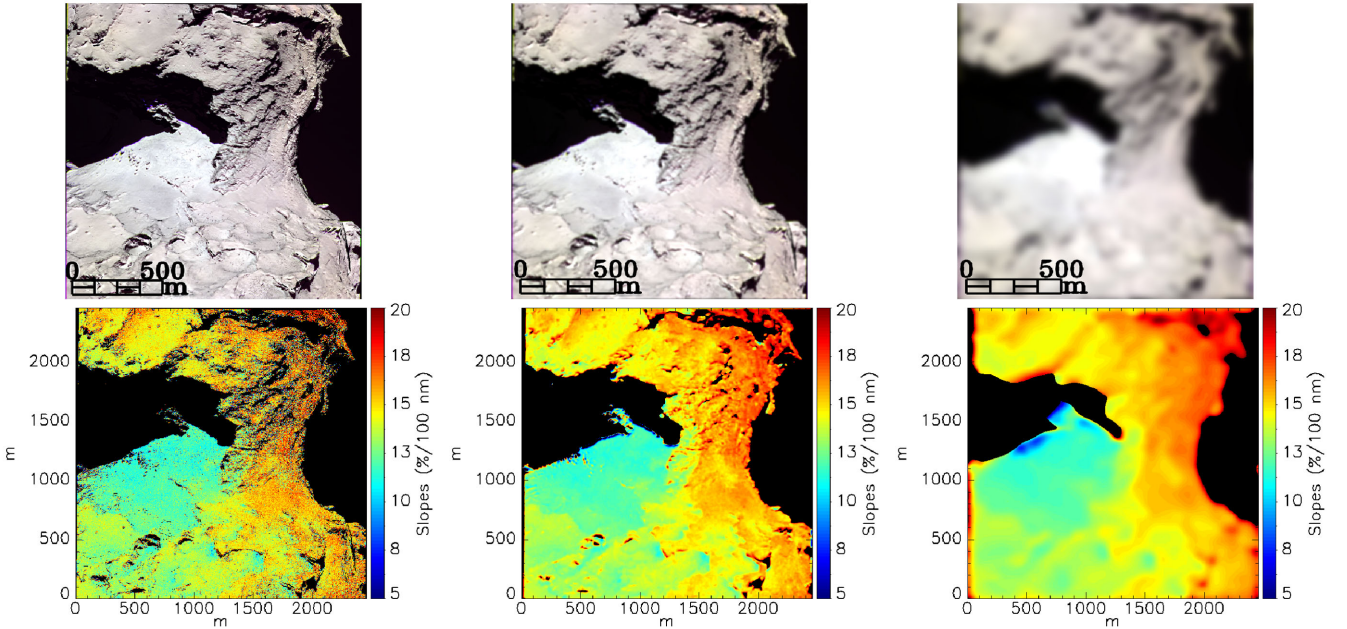
The NAC image sets #1–3 (Table 1) in *DI*-HRI spatial resolution are given in the left-hand column of Fig. 4 (from top panel to the bottom, respectively) with selected ROIs overlaid. The corresponding relative reflectance calculated per ROI (see Section 3 for details) is plotted together with the relative reflectance of the water ice deposits given in Sunshine et al. (2006) for comet 9P and in Sunshine et al. (2011) for comet 103P in the right-hand column of Fig. 4. The ROIs selected on comets 9P and 103P images are displayed in Fig. B2. On comet 67P, the water-ice-rich cluster BAP2 of Filacchione et al. (2016c) are ROIs #4 and #1 in image set #1 and #2, respectively (left-hand column, top two panels of Fig. 4). The water-ice-rich cluster BAP1 of Filacchione et al. (2016c) is ROI #1 in image set #3 (bottom-left panel of Fig. 4). ROI #2 in set #1 (top-left panel of Fig. 4) and ROI #5 in set #2 (middle-left panel of Fig. 4) are the water-ice-rich spots 7 and 5 of Barucci et al. (2016), respectively. All other ROIs in the images represent potentially water-ice-rich features, except for the ones indicating average surface (the ROI with the largest # in each data set). The relative reflectance values

of water-ice-rich and potentially water-ice-rich features decrease with increasing wavelength, i.e. the spectra have blue slopes in all image sets (right-hand panels of Fig. 4). This spectral behaviour was used as a diagnostic tool for the detection of water ice deposits on the surface of comets (Sunshine et al. 2006, 2011). The comparison of spectral properties of selected features (ROIs) shows that the ROI#4 (large isolated potentially water-ice-rich feature), ROI#5 (the water-ice-rich feature) in set#2 (middle-right panel of Fig. 4) and ROI#8 (small potentially water-ice-rich isolated feature) in set#3 (bottom-right panel of Fig. 4) of comet 67P have bluer spectra than the other selected features of comet 67P. Additionally, these large isolated features have bluer spectra than the water ice deposits seen on comet 9P. However, the large water ice deposit observed on comet 103P has the bluest spectra indicating higher water ice abundance than the other investigated features. The same was concluded by Sunshine et al. (2011) as a result of IR spectroscopic analysis of the water ice deposits observed on comets 9P and 103P. Water-ice-rich clusters BAP2 (represented in ROI#4 in set#1, and ROI#1 in set#2) and BAP1 (represented in ROI#1 in set#3) have very similar spectra to the water ice deposits observed on comet 9P indicating similarities in the physical properties of those features observed in both comets.

The NAC image sets in *DI*-MRI spatial resolution are given in the left-hand panels of Fig. 5 with selected ROIs overlaid. The relative reflectances calculated per ROI (see Section 3 for details) are plotted together with the relative reflectances of the water ice deposits given in Sunshine et al. (2006) for comet 9P. On comet 67P, water-ice-rich cluster BAP2 is seen in ROIs #3 and #1 in image sets #1 and #2, respectively (left-hand column, top two panels of Fig. 5). The water-ice-rich cluster BAP1 is ROI #1 in image set #3 (bottom-left panel of Fig. 5). All other ROIs in the images represent potentially water-ice-rich features except for the ones indicating average surface (the ROI with the largest # in each data set). Here, we note that less features could be detected in this spatial resolution. Therefore, the image sets are investigated in few ROIs. The comparison of spectral properties of selected features shows that in this spatial resolution both isolated and clustered bright features have very similar spectra (right-hand panels of Fig. 5). As expected from the results of the same analysis performed in *DI*-HRI resolutions, all selected ROIs (left-hand panels of Fig. 5) have very similar spectra to the water ice deposits observed on comet 9P at the wavelengths longer than 550 nm. At shorter wavelengths, deviations can be explained by the large errors in the *DI*-MRI data.

3.2 Comparison of water ice patches with Hapi region of comet 67P

Hapi is a region between the two lobes of comet 67P. This large smooth region was the most active, displaying many jets at the arrival of *Rosetta* spacecraft to the comet 67P on 2014 August. Similar to the water ice deposits, the Hapi region has high albedo (Fornasier et al. 2015b), and displays light blue colour in the RGB images prepared using images taken with filters centred at NIR, visible and NUV wavelengths (top panel of Fig. 6). This region has lower spectral slopes (bottom panel of Fig. 6) comparable to the values of water ice and potentially water ice features (Oklay et al. 2016). This comparison is done by assuming no spectral reddening between the phase angles of the investigated images. The same assumption was safely used by Oklay et al. (2016) since the spectral slope variation in phase angles 34°–54° is negligible (see Fornasier et al. 2015b, fig. 3). As a result of the spectral analysis of comet 67P's surface, Hapi region was identified to have high water

Figure 6. Colour composites (top panels) and corresponding spectral slopes (bottom panel) of Hapi region at original NAC resolution in left-hand panels, *DI*-HRI resolution in middle panels and *DI*-MRI resolution in right-hand panels. Images taken in 989.3, 649.2 and 360.0 nm are assigned to the RGB channels of the top panel images, respectively.

abundance (Fornasier et al. 2015b). By the multispectral imagers of the previous comet missions, this region would be detected as a large water ice deposit due to its low spectral slopes. Similarly, active pits and alcoves seen in the same image set (see fig. B2 of Oklay et al. 2016, for the features) would be detected as water-ice-rich features. Multispectral properties of Hapi, active pits and the alcoves seen in this image set are very similar (see fig. 4 b of Oklay et al. 2016). Moreover, the multispectral properties of Hapi region are similar to the water ice features (see fig. 13 of Oklay et al. 2016). Therefore, the Hapi region is included in our comparative analysis.

Photometrically corrected and co-registered multispectral data of the colour set labelled with 67P-NAC-Hapi ID in Table 1 are presented using colour composites at the top panels of Fig. 6 in NAC, *DI*-HRI and *DI*-MRI resolutions from left to right, respectively. Images taken at 989.3, 649.2 and 360.0 nm are used in the RGB channels of the images, respectively. Corresponding spectral slopes are given in the bottom panels of Fig. 6. The Hapi region has a mean spectral slope value of 10 per cent/100 nm in the images taken in NAC resolution, while the mean spectral slope value in *DI*-HRI and *DI*-MRI resolutions is 12 per cent/100 nm. These low spectral slope values correspond to the active regions (Oklay et al. 2016) on the surface of comet 67P. Indeed, numerous jets are visible once the images are stretched (see fig. B1 of Oklay et al. 2016). The low spectral slopes at the bottom of pits and alcoves are also notable. Associated activity features observed in OSIRIS NAC images are given in Oklay et al. (2016, fig. B2). Spectral properties of the activity sources seen in this image set were investigated by Oklay et al. (2016) and the spectral similarities of the active regions with water-ice-rich features were presented. Therefore, in this study we only focus on the comparison of Hapi region with the water ice deposits observed on comets 9P and 103P.
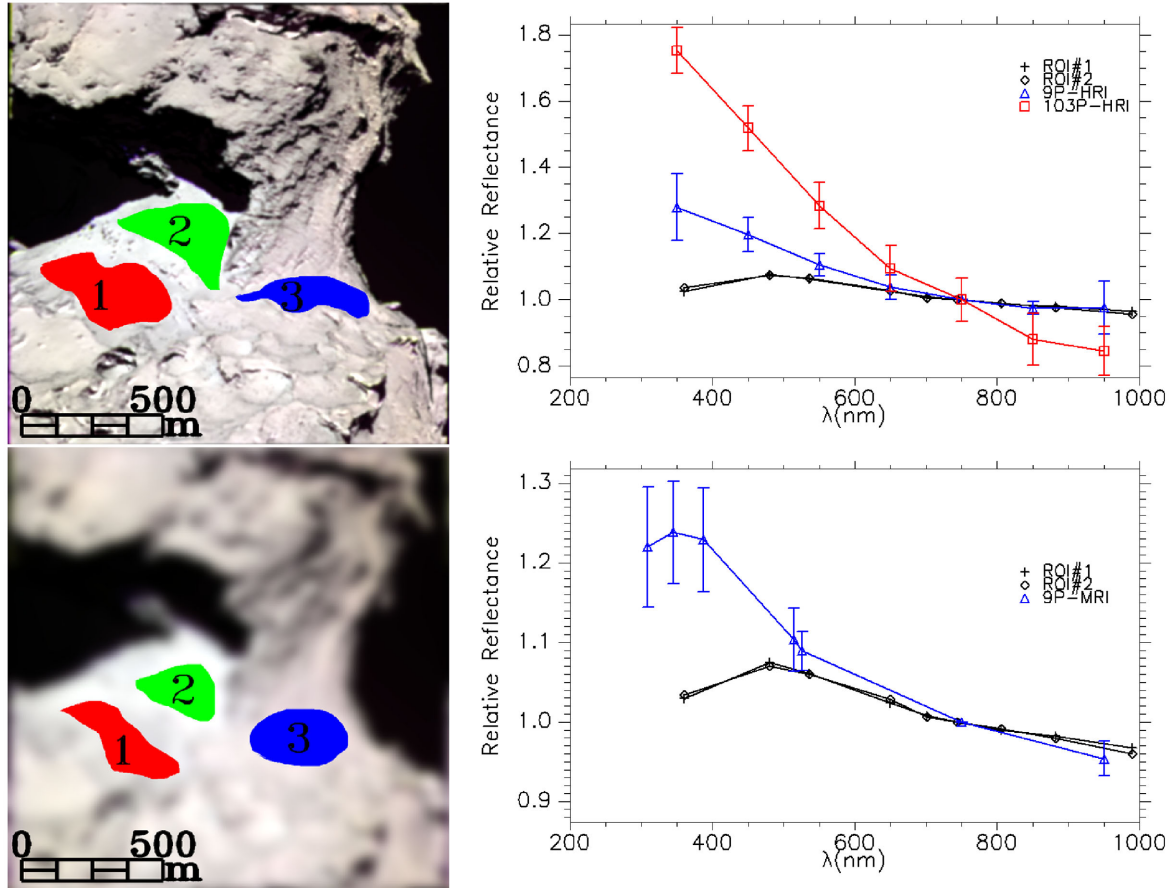
The ROIs selected on OSIRIS NAC images in *DI*-HRI and *DI*-MRI spatial resolutions are presented in the left-hand column of

Fig. 7 from top to bottom, respectively. There are three ROIs defined per image. Investigating wide smooth Hapi region in two ROIs is to avoid the large boulders present in the region. The ROIs #3 in each image represent the average surface used in the surface normalization. The relative reflectance of each ROI per image (see Section 3 for details) is plotted together with the relative reflectance of water ice deposits observed on comet 9P (Sunshine et al. 2006) and comet 103P (Sunshine et al. 2011). Hapi spectrum has blue slope in 500–1000 nm wavelength range, similar to the water-ice-rich features seen on the surface of comet 67P. This is in good agreement with the spectra of water ice deposits seen on comet 9P (right-hand panels of Fig. 7) in this wavelength range. The disagreement in the wavelengths below 480.7 nm is probably due to the coma contribution seen on comet 67P images at that wavelength. The coma contribution in NAC spectrum at specific filters is discussed in Fornasier et al. (2015b) and in Oklay et al. (2016). The water ice deposit observed on comet 103P has the bluest slopes, interpreted as higher water ice abundance.

3.3 Locations of water ice deposits and their potential origin

The locations of water-ice-rich features, morphological features in their vicinity, blue bright boulder size–frequency distributions and multispectral imaging allow us to investigate their possible origin and how they were exposed to the surface.

Four water ice deposits (marked in blue at the top panel of Fig. B2) detected on the surface of comet 9P have total area of 0.5 km^2 (Sunshine et al. 2006). The two large ones have about 350 m diameter, while the other two have diameters of about 100 m each. These deposits are located in depressions (Sunshine et al. 2006). The large water ice deposit (blue rectangle in the bottom panel Fig. B2) observed on comet 103P has a diameter of about 150 m and is located in a rough terrain near along the terminator. As described in
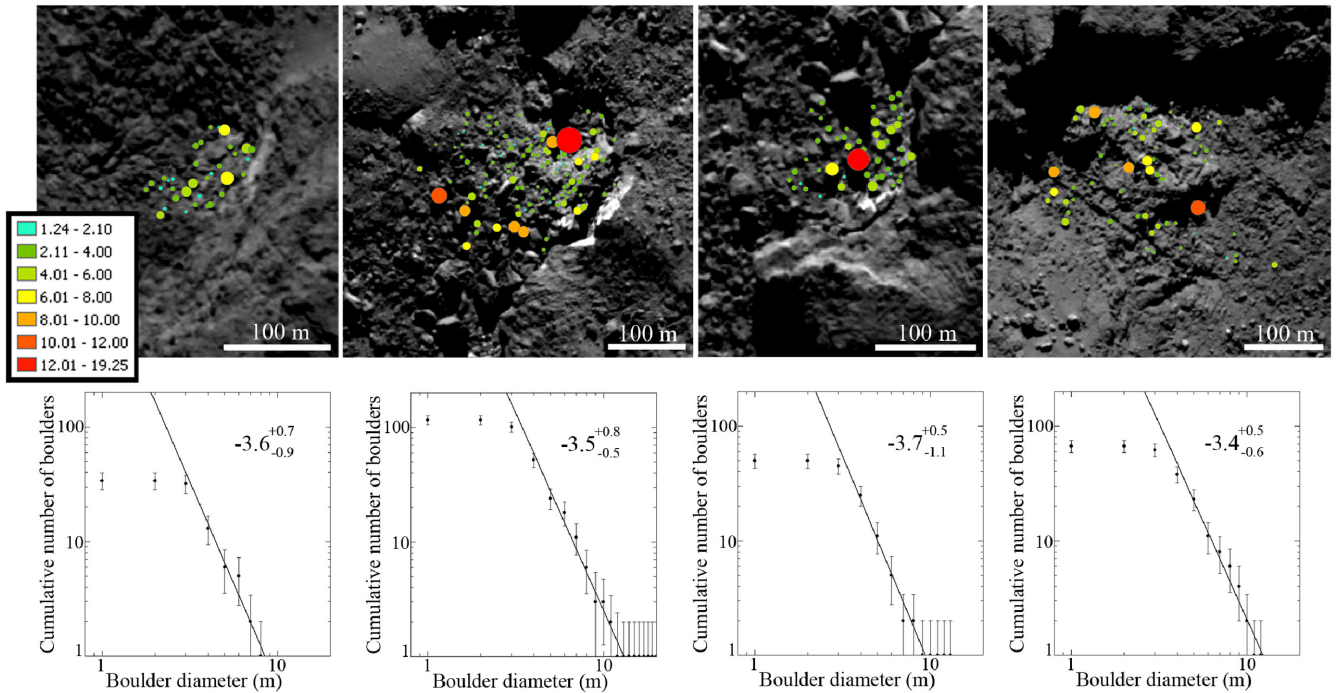
Figure 7. Selected ROIs on NAC image set (left-hand column) in *DI*-HRI (top panel) and *DI*-MRI (bottom panel) spatial resolutions. Corresponding relative reflectance is given in the right-hand column together with the spectra of water ice deposits observed on comets 9P and 103P. Typical standard deviation of the data points in the top panel are 4.45×10^{-6}, while it is 2.80×10^{-6} for the data points in the bottom panel. ROI#3 in both images represent the average surface, where the mean spectra of each ROI are normalized (see Fig. B3 for the spectra).

Section 3.1, large clustered water-ice-rich features observed on comet 67P are located by the cliffs and isolated ones are located below overhangs.

On comet 67P the two large clusters, where the water ice was detected (features #2, 4 in Table A1), are about 100 m wide along their neighbouring cliff with debris fields extending up to 150 m away from their neighbouring cliff (see second and fourth top panels of Fig. 8). The smaller cluster (feature #5) in the neighbourhood of feature #4 (Table A1) is almost as wide as the large clusters with a debris field up to about 65 m (third top panel of Fig. 8). However, the small cluster (feature #16 in Table A1) is about 75 m wide along its neighbouring cliff with a debris field extending about 50 m (top-left panel of Fig. 8). These measurements show that the dimensions of the water-ice-rich clusters are comparable to the small water ice deposits observed on comet 9P and the water ice deposit observed on comet 103P. The location of the ice deposits on all three comets appear to be heavily influenced by topography. The deposits on comet 9P are in depressions and those on comet 103P are in rough terrains both of which suggest that local topographic shadowing could play a role in preservation. On comet 67P, the higher resolution data suggest down-slope movement exposing fresh materials. The water-ice-rich boulders observed on the investigated images of comet 67P have sizes up to 20 m (top panels of Fig. 8), whereas the large isolated water-ice-rich features have diameters between 4 and 13 m (Fig. 9).

High spatial resolution multispectral imaging of comet 67P allows us to detect colour variations of water-ice-rich features in the case of Hapi region where condensation of water ice was observed and the bright blue features where water ice was observed. Moreover, using such images we detected bright blue edged cliffs above their taluses containing water ice. This is a clear evidence of a cliff collapse and exposure of water ice from beneath the subsurface. However, using bright boulder size–frequency distributions, we are able to detect cliff collapse associated water ice exposures without the detection of blue edged cliffs.

Cumulative size–frequency distribution (Section 2.3) is indicative of the formation and evolution processes of the considered boulders and provides a geomorphological context to their origin. Since comet 67P is the only comet where the water ice could be detected in small scales within clusters, we applied it to the bright blue boulders. By using three reference (taken at 701.2 nm) NAC images obtained on 2014 September 5 at 05:31, 06:36 and 06:46 UT, respectively (all with a scale of 0.76 m px^{-1}, see Table 1), we had the possibility to perform a similar bright boulder computation to the one that was done in Pommerol et al. (2015b). Indeed, on four different clusters, #16, #4, #5 and #2 (Table A1), several tens of bright patches permitted to retrieve meaningful size–frequency distributions and the corresponding power-law indices. Within such clusters, it was not possible to properly extract the extension of the areas containing them from the comet 67P shape

Figure 8. Water-ice-rich boulder sizes within the water-ice-rich clusters detected on the surface of comet 67P (top panel). Sizes of the boulders are colour coded and the values are given in the labels in each panel. The size–frequency distribution of the water ice boulders is given in the bottom panel. The features #16, #4, #5 and #2 are displayed from left-hand panel to the right-hand panel, respectively. The locations of these features on the images are given in Fig. B1 and their coordinates are given in Table A1.

Figure 9. Isolated boulder sizes and areas. Left-hand panel shows the feature #14, which contains (Barucci et al. 2016, spot7), second panel from the left shows the features #12E, #12W (Barucci et al. 2016, spot 5), #13 and second panel from the right-hand panel shows the feature # 1 (left-hand panel) and #3 (right-hand panel). The locations of these features on the images are given in Fig. B1 and their coordinates are given in Table A1.

model, and hence we did not get the cumulative number of boulders per km^2. Nevertheless, the power-slope index of the size–frequency distribution is independent from areas, therefore it is still diagnostic of the related formation processes (Pajola et al. 2015).

Despite the different maximum sizes identifiable on the four clusters, all of them present a comparable power-slope index, falling inside, or in close proximity, to the type II range (Pajola et al. 2015). This range, between -3.5 and -4.5, was observed on multiple areas of comet 67P, always associated with deposits located in close proximity or, at the foot of the cliffs. The possible interpretation of the surface processes which lead to this power-slope index is presented in Pajola et al. (2015) and Pajola et al. (2016b, fig. 8), and is here summarized.

After pits are formed[8] on the surface of the comet through escape of high-pressure volatiles and fracturing, thermal stresses and heat affect the exposed interior of the comet, possibly forming new fractures inside the cometary mixture of ice and dust. This results in sublimation from the newly formed walls of the pit or the boulder field below. While the fracturing increases, repeated sublimation occurs on the cliff, eroding its shape. The consequence

---

[8] Independently if there is a primordial void, remnant of the comet formation, or a subsurface heat source which sublimates the surrounding ices consequently forming a cavity, when surface erosion lowers the upper layer above the void, it favours, at some point, the ceiling to collapse. The consequence of this is that a circular pit is formed, with a boulder field at its bottom (Pajola et al. 2016b).

of this is that the cliff retreats, gravitational events occur and a boulder field at the foot of the cliff is formed. Multiple cases of boulder fields located at the foot of retreating cliffs, imaged with minimum scales ranging between 0.5 m (Vincent et al. 2016) and 2.3 m (Pajola et al. 2015), have been observed on comet 67P, all presenting this diagnostic power-slope index ranging between −3.5 and −4.5. Since the power-slope index we derive for such bright deposits is totally comparable with the above values, we believe that such clusters, characterized both by bright and dark boulders, were once constituting the surrounding cliffs retreated with time. One more hint which strengthens this interpretation is that the bright ice patches observed in this work are not only located below the cliffs, but also on overhangs edges, that are possibly prone to fall.

On the contrary, due to the small number of boulders present in the localized bright areas, it was not possible to perform a size–frequency analysis and to derive a meaningful power-law index (features #14, #12E, #12W, #13, #1 and #3, Table A1). However, their sizes and corresponding area have been computed and presented in Fig. 9.

There are bright blue features in sizes between 70 cm up to few tens of metres on the surface of comet 67P (Pommerol et al. 2015b). However, the sizes of individual surface features are limited with the spatial resolution of the images. Therefore, the lower limit for the water-ice-rich boulders can change once a better spatial resolution is achieved during observations.

3.4 Temporal evolution of the ice patches

The observations of comets 9P and 103P were flybys, not suited for a long-term temporal study of the water ice deposits seen on their nuclei. However, such analysis is possible for the water-ice-rich features on the surface of comet 67P. Pommerol et al. (2015b) reported no temporal variation on the bright features within a time period of two weeks, and some of the bright features investigated by Barucci et al. (2016) were stable up to 15 weeks. Due to operational constrains on the *Rosetta* spacecraft trajectory, there are no systematic observations of water-ice-rich features in high spatial resolutions. In the low spatial resolution images, it is challenging to study the multispectral properties of such features seen in Fig. B1 during the observations taken in 2015. However, we started to observe the extended Imhotep region in high spatial resolutions again at the beginning of 2016, and the data given in Table 2 are used to detect the variation of the water-ice-rich features over ≈1.5 yr time.

A visual comparison of water-ice-rich features seen on the surface of comet 67P is presented in Fig. 10 at two different epochs. In the left-hand column, the enriched water ice features are seen on 2014-09-05, while in the right one they are seen on 2016-01-24. The large blue debris fields (see Section 3.3 for details) seen in the top two left-hand panels of Fig. 10 are almost completely vanished due to sublimation of existing water ice during this period of time. Some water ice still remains at the locations very close to neighbouring cliff. The water ice within the cluster seen in the second panel from the top of Fig. 10 is completely sublimed during this period of time. The water ice seen in the two isolated blue features (Fig. 10, second panel from the bottom) is surprisingly not completely sublimated over this time. Not all blue features (enriched in water ice) have vanished, but some appeared in between these observations. At the bottom panel, the variation around the roundish features is presented. Those regions were identified as active in Oklay et al. (2016) and they became bluer during the time of 1.5 yr. The green colour detected earlier around the roundish features was possibly
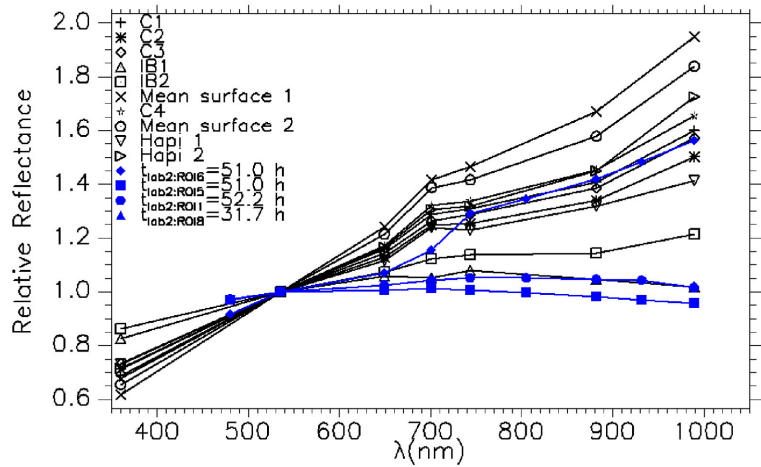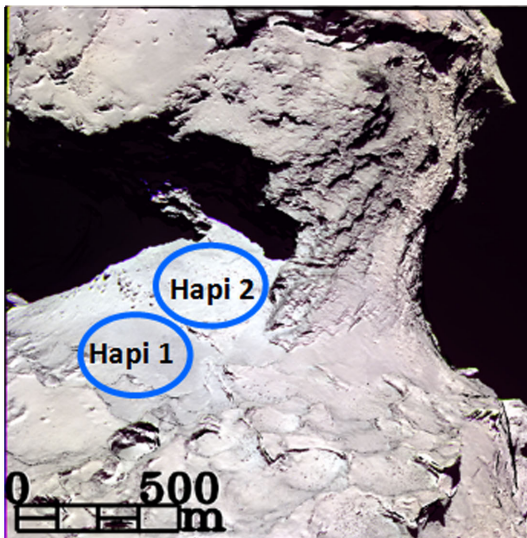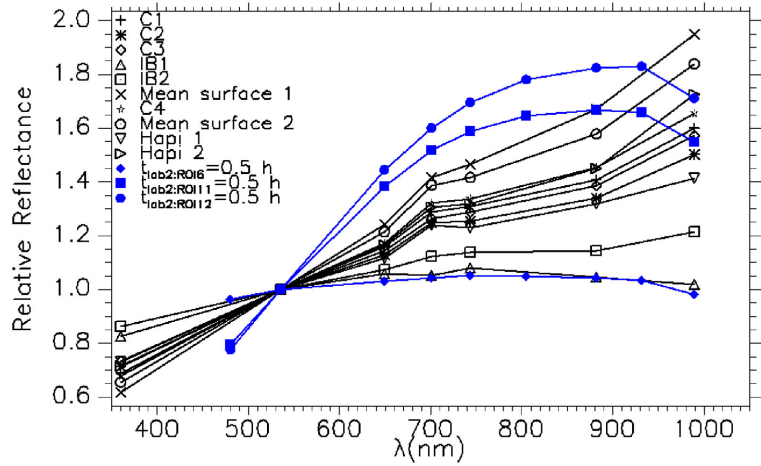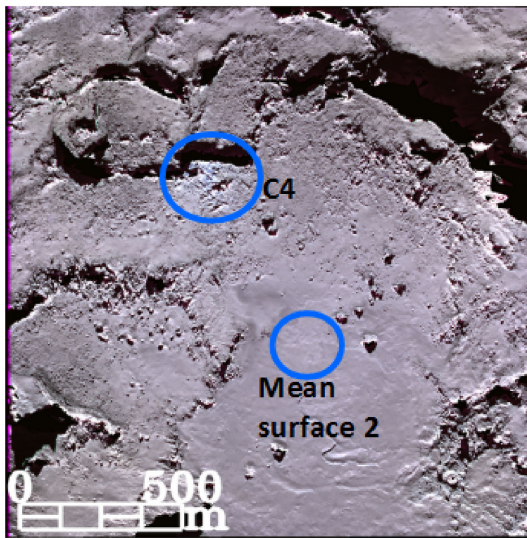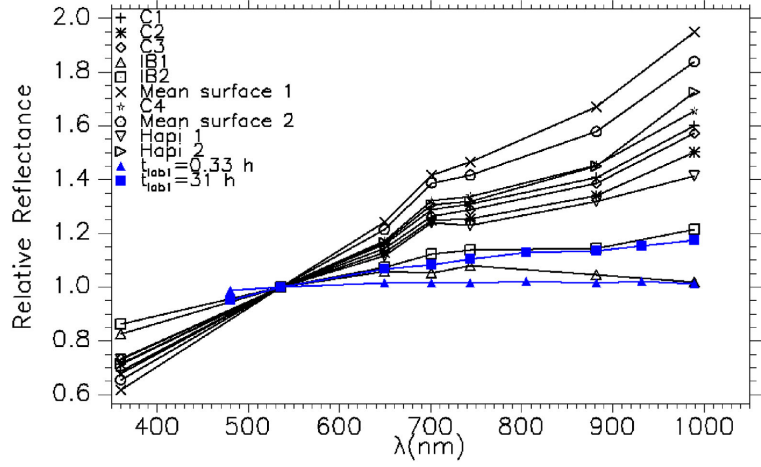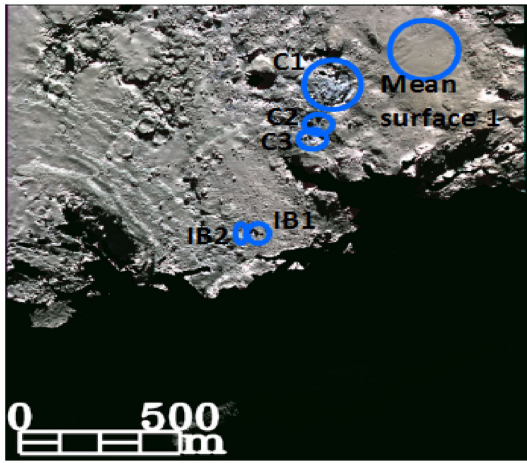

Figure 10. Comparison of the water-ice-rich features observed at two different epochs (Table 2). The images in the left-hand panel are taken on 2014-09-05, while the images in the right-hand panel are taken on 2016-01-24. Images taken in 882.1, 649.2 and 480.7 nm filters are used to generate colour composites. Histogram match stretch is applied to the image pairs. Top two panels are the water-ice-rich clusters BAP2 (top panel) and BAP1 (second panel) of Filacchione et al. (2016c). Third panel from the top shows one potentially water-ice-rich (upper) and one water-ice-rich (lower) feature (Barucci et al. 2016, spot 5). Bottom panels show the roundish features and their surrounding material.

due to the dust covering the water ice beneath. Comet 67P passed its perihelion in between these two observations, where its activity was increased significantly. It might be that the dust covering the water ice might be removed and allowed the detection of the water ice below. The detailed analysis on the temporal variation of water-ice-rich and potentially water-ice-rich features is an ongoing work (Oklay et al. in preparation).

3.5 Results obtained using laboratory experiments

The mean spectra of water-ice-rich features observed on comet 67P (left-hand panels of Fig. 11) and the mean spectra of Hapi region are compared with the resampled laboratory data of Pommerol et al. (2015a, µm-sized water ice, carbon black and airfall volcanic dust) using spectra normalized[9] at 535.7 nm (top-right panel of Fig. 11). The mean surface spectrum of comet 67P is included to the comparison as a reference. Water-ice-rich clusters C1 and C4 correspond to BAP2 and BAP1 in Filacchione et al. (2016c), respectively, while IB2 is spot 5 of Barucci et al. (2016). The laboratory data show a very flat spectrum at the beginning of the sublimation experiment, in good agreement with the mean spectrum of IB1, whereas

---

[9] As described in Section 3, no surface normalization is applied in this analysis.

Figure 11. Comparison of water-ice-rich features with the laboratory experiments of Pommerol et al. (2015a) and Poch et al. (2016). Left-hand panels display the surface features used in the comparison. Right-hand panels show the comparison of laboratory data with the mean spectra of the features displayed in the top panels. See the text for details.

the spectrum at the end of the sublimation resembles the spectrum of IB2. The mean spectra of water-ice-rich clusters (C1, C4) show redder spectral slopes than these particular laboratory spectra, probably due to the large amount of organic material at the surface of comet 67P and a broader range of compositions compared to the pure carbon used in the experiment.

Resampled spectra for all ROIs given in Poch et al. (2016, water ice mixed with tholins and minerals) are compared as well with the mean spectra of the features displayed in Fig. 11. Spectra normalized at 535.7 nm are used for this comparison. The mean spectra of ROIs 1–5, 7–10 at the beginning of the sublimation experiment are not representative of the mean spectra of the features we investigate (Fig. A2). This is expected, as the laboratory experiments begin with much larger ice to dust ratios than what is found on the comet, even over ice-rich patches. Therefore, only the relevant spectra extracted from the laboratory spectral time series are shown in the right-hand panels of Fig. 11 together with the mean spectra of the features we are interested in.

The comparison performed using different mixtures studied by Poch et al. (2016) shows that in the case of a water ice–olivine mixture, the spectra of ROI1 and ROI8 at the end of the sublimation experiment are both very similar to the mean spectrum of IB1 (bottom-right plot of Fig. 11). Towards the beginning of the experiment, ROI6 shows a similar spectrum to IB1 (middle-right plot in Fig. 11), but it becomes more similar to the observed spectra of water ice clusters at the end of the sublimation experiment. The mixtures with tholin (ROIs 11 and 12 in the middle-right plot of Fig. 11) show redder spectral slopes than the mean surface spectra at the beginning of the experiment. The tholins used in the experiments are much redder than the organic material found at the surface of the comet. Although none of the dust components used in the laboratory experiments are completely representative of the dust found at the surface of the nucleus, the comparison already shows that the observed variability in the visible spectra observed at the surface of the comet can be explained by the progressive sublimation of water ice from an ice/dust mixture. Additional experiments will be required to find a good spectral analogue of the nucleus surface in the visible spectral range. It is also clear that it is only by combining the constraints provided by different spectral ranges that firm and quantitative conclusions will be reached on the nature and amount of volatile and refractory elements at the surface of the comet.

The physical properties of the laboratory mixtures given at the bottom panels of Fig. 11 are:

(i) Lab1 (Pommerol et al. 2015a): comet 1 run (ROI1): water ice (4.5 µm) + carbon black (42 nm, 1 wt per cent) and fine volcanic ash (5 wt per cent)

(ii) Lab2 (Poch et al. 2016):

(a) ROI1 (intra mixture): water ice (67 µm) + olivine($\leq$ 80 µm, 1 per cent),
(b) ROI5 (intra mixture): water ice (67 µm) + smectite($\leq$ 80 µm, 1 per cent),
(c) ROI6 (inter mixture): water ice (67 µm) + smectite($\leq$ 80 µm, 1 per cent),
(d) ROI8 (inter mixture): water ice (67 µm) + smectite($\leq$ 80µm, 0.1 per cent).

4 CONCLUSIONS AND OUTLOOK

Multispectral imaging from NUV to NIR wavelengths allows reliable detection of water-ice-rich and potentially water-ice-rich fea-tures on comet nuclei due to their blue colour. The potentially water-ice-rich features detected using such RGB images can then be investigated in the IR wavelengths for the confirmation of water ice and derivation of their physical properties.

The detection and quantitative comparison of various surface units requires normalized techniques such as determination of spectral slopes or image ratios. Therefore, spectral slopes calculated using only two images taken in NUV and NIR wavelengths is an independent tool of detecting surface variegation including water-ice-rich and potentially water-ice-rich features on comet 67P. Such a method has the advantage of being used during imaging with limited number of filters, when full spectral analysis cannot be performed. While the visible slope is not diagnostic of water ice, data from three comets now provide strong indications that multispectral imaging can be used to identify likely areas of water ice enhancement. Depending on their goals, future missions which wish to identify water-ice-rich regions on cometary surfaces are likely to safely do so based on colour slope. Low spectral slope values of the water-ice-rich and potentially ice rich features (Fig. 2) indicate that they belong to the active surface region group defined by Oklay et al. (2016). Indeed, associated jets and outburst to these features are observed when the right observing conditions were fulfilled.

Spectral properties of some bright blue features observed on comet 67P were investigated and compared with laboratory experiments of the water ice mixtures (Pommerol et al. 2015b; Oklay et al. 2016). After such analysis, water ice was found to be the most plausible explanation to explain the blue nature of the features seen on the surface of comet 67P. Further investigations of these features in IR wavelengths revealed the existence of water ice. Therefore, we conclude that the potentially water-ice-rich features investigated in this study are actually water-ice-rich features. If the spectrometer on board *Rosetta* spacecraft has data on the features given in Table A1, further investigation in IR wavelengths will confirm our findings obtained from the visible wavelengths. Moreover, activity features (i.e. jets, outbursts) were observed in some of the water ice patches (see Oklay et al. 2016, for examples). Most of these activity detections were about half a year after the detection of these blue features. These late detections were probably due to more suitable observing geometries allowing such detection. Therefore, activity features can be detected from the investigated features in future observations.

Our multispectral analysis on water-ice-rich features concludes that the water ice deposits observed on comet 9P are similar to the clustered water-ice-rich features observed on comet 67P, while the water ice deposits observed on comet 103P are similar to the large isolated water-ice-rich features seen on comet 67P. As a result of our comparative study, we conclude that isolated water-ice-rich features observed on comet 67P contain more water ice than the ones observed on comet 9P, but none of the water-ice-rich or potentially water-ice-rich features on comet 67P have as much water ice as the brightest water ice patch observed on comet 103P. However, the comparison of absolute amount of water ice for each comet requires analysis that go beyond what can be achieved with the currently available data sets.

Our investigation on the size and location of the water ice deposits observed on comets 9P, 103P and 67P shows that those deposits have similar sizes and their locations seem to be influenced by local topography. In the case of comet 67P, the blue edges of the neighbouring cliff suggest cliff collapse as their surface exposure.

Spectral slopes of the laboratory data are significantly higher than the ones observed on the surface of comets (Poch et al. 2016, fig. 6). This is due to the spectral properties of the dust species considered during the experiments. However, the comparison done using the

relative reflectance shows that some of the laboratory setups have comparable spectra to the observed water-ice-rich features. Our analysis shows difficulty in distinguishing between some of the experimental setups in the visible wavelengths.

Properties of water-ice-rich features detected using multispectral data in the 260–1000 nm range are as follows.

(i) Water-ice-rich features appear bright in monochromatic images.

(ii) Water-ice-rich features are blue in the image composites generated by using images taken in IR, visible and UV wavelengths.

(iii) Clustered water-ice-rich features have similar spectral features as the average comet surface but have bluer spectra, while isolated water-ice-rich features have flat spectra.

(iv) Some of the water-ice-rich features are the source of activity features (jets, outbursts).

(v) Water-ice-rich features have spectral slopes of 5–13 per cent/100 nm.

Quantitative results, i.e. sublimation rates, lifetimes and thickness of the water ice observed on the surface of comets can be determined only for comet 67P where observations of water-ice-rich features are available over time. Such analysis is in progress for the water-ice-rich features seen on comet 67P, including long-term observations before and after perihelion (Oklay et al. in preparation).
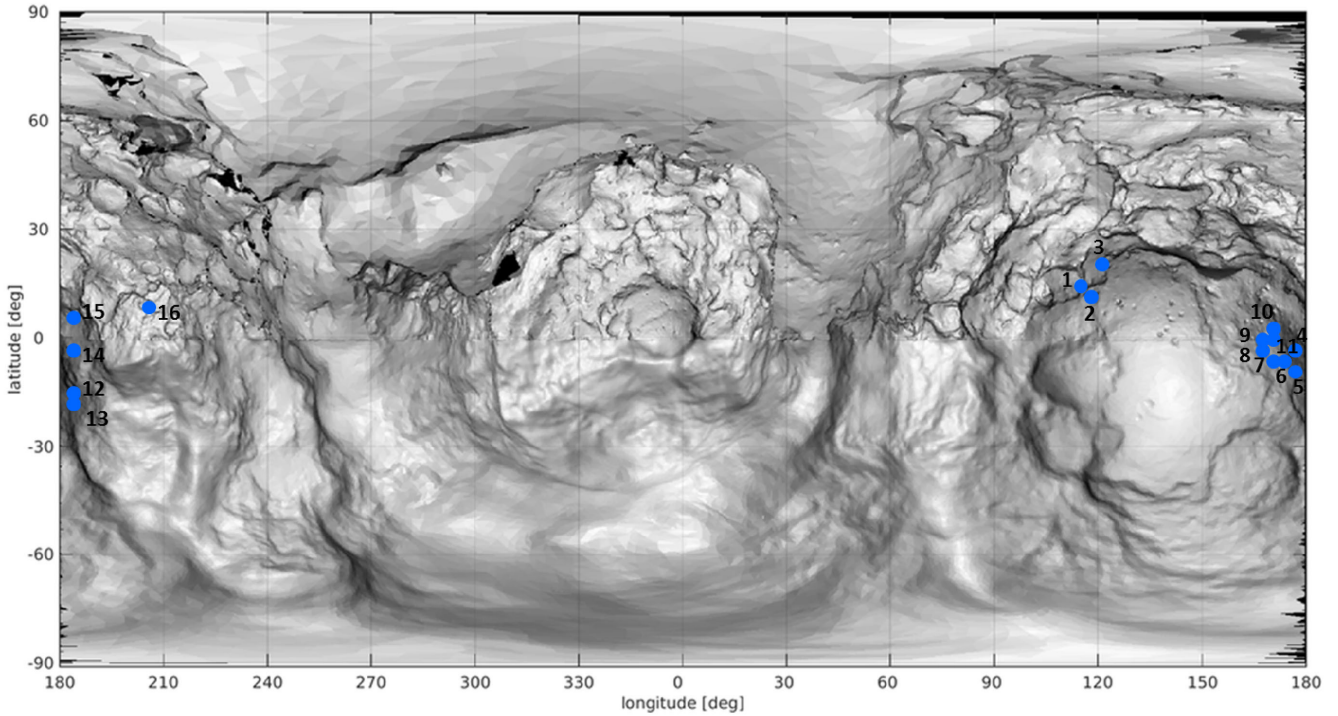
ACKNOWLEDGEMENTS

REFERENCES

A'Hearn M. F. et al., 2005, Science, 310, 258
A'Hearn M. F. et al., 2011, Science, 332, 1396
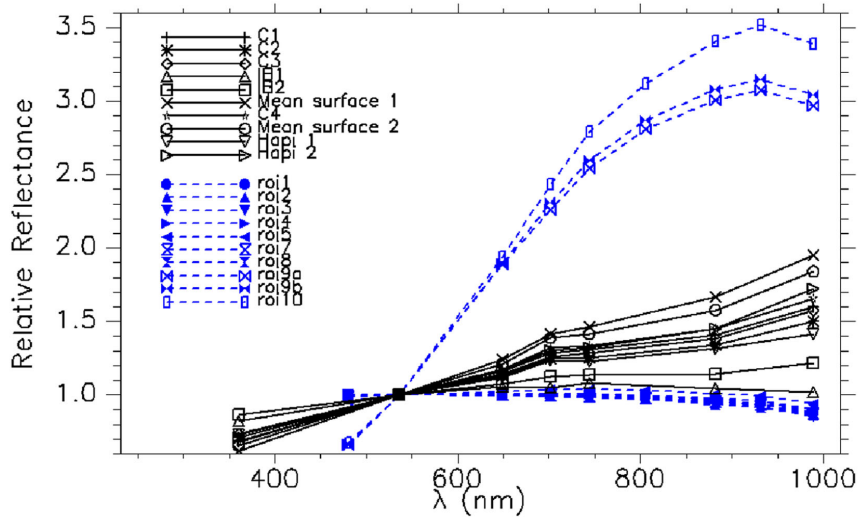Anderson J. A., Sides S. C., Soltesz D. L., Sucharski T. L., Becker K. J., 2004, in Mackwell S., Stansbery E., eds, Lunar Planet. Sci. Conf. Tech. Rep. Vol. 35, Modernization of the Integrated Software for Imagers and Spectrometers. p. 2039
Barucci M. A. et al., 2016, A&A, 595, A102
De Sanctis M. C. et al., 2015, Nature, 525, 500
El-Maarry M. R., Thomas N., Gracia-Berná A., Pajola M., The OSIRIS Team, 2016, A&A, 593, A110
Filacchione G. et al., 2016a, Science, aag3161
Filacchione G. et al., 2016b, in EGU General Assem. Conf. Abstr. p. 11930
Filacchione G. et al., 2016c, Nature, 529, 368
Fornasier S. et al., 2015a, in AAS/Division for Planetary Sciences Meeting Abstracts. p. 500.06
Fornasier S. et al., 2015b, A&A, 583, A30
Fornasier S., Mottola S., Keller H. U., Barucci M. A., Davidsson B., The OSIRIS Team, 2016, Science, aag2671
Glassmeier K.-H., Boehnhardt H., Koschny D., Kührt E., Richter I., 2007, Space Sci. Rev., 128, 1
Hampton D. L., Baer J. W., Huisjen M. A., Varner C. C., Delamere A., Wellnitz D. D., A'Hearn M. F., Klaasen K. P., 2005, Space Sci. Rev., 117, 43
Hapke B., 1993, Theory of Reflectance and Emittance Spectroscopy, 1st edn. Cambridge Univ. Press, Cambridge
Jorda L. et al., 2016, Icarus, 277, 257
Keller H. U. et al., 2007, Space Sci. Rev., 128, 433
Klaasen K. P. et al., 2008, Rev. Sci. Instrum., 79, 091301
Klaasen K. P. et al., 2013, Icarus, 225, 643
Knollenberg J. et al., 2016, A&A, 596, A89
La Forgia F. et al., 2015, A&A, 583, A41
Li J.-Y. et al., 2007, Icarus, 187, 41
Li J.-Y. et al., 2013, Icarus, 222, 559
Lindler D., Busko I., A'Hearn M. F., White R. L., 2007, PASP, 119, 427
Lucchetti A. et al., 2016, A&A, 585, L1
Nyquist H., 1928, Trans. Am. Inst. Electr. Eng., 47, 617
Oklay N. et al., 2015, A&A, 583, A45
Oklay N. et al., 2016, A&A, 586, 18
Pajola M. et al., 2015, A&A, 583, A37
Pajola M. et al., 2016a, A&A, 585, A85
Pajola M. et al., 2016b, A&A, 592, A69
Poch O., Pommerol A., Jost B., Carrasco N., Szopa C., Thomas N., 2016, Icarus, 267, 154
Pommerol A., Jost B., Poch O., El-Maarry M. R., Vuitel B., Thomas N., 2015a, Planet. Space Sci., 109, 106
Pommerol A. et al., 2015b, A&A, 583, A25
Preusker F. et al., 2015, A&A, 583, A33
Sierks H. et al., 2015, Science, 347, aaa1044
Sunshine J. M. et al., 2006, Science, 311, 1453
Sunshine J. M. et al., 2011, Water Ice on Comet 103P/Hartley 2. p. 1345
Taylor M. G. G. T., Alexander C., Altobelli N., Fulle M., Fulchignoni M., Grün E., Weissman P., 2015, Science, 347, 387
Vincent J.-B. et al., 2016, A&A, 587, A14

APPENDIX A: LOCATION OF INVESTIGATED SURFACE FEATURES ON COMET 67P

The location of water-ice-rich and potentially water-ice-rich features detected on the investigated images of comet 67P (Table 1) are presented in Fig. A1. Coordinates, type and area of these features are given in Table A1 together with the references for the water ice confirmation if there is any. Investigated images (Table 1) cover extended Imhotep region. Therefore, the locations of the features are logically concentrated in this region. The images used in the temporal variation analysis show exposure of new potentially water-ice-rich features more on the southern Imhotep region (Oklay et al. in preparation).

Figure A1. Distribution of the water-ice-rich and potentially water-ice-rich features (blue dots) on the surface of comet 67P in the image sets given in Table 1. This map is a cylindrical projection of combined shape models of Preusker et al. (2015) for the Northern hemisphere and of Jorda et al. (2016) for the Southern hemisphere. The top of the small lobe is at about 0°, 0°(in the middle), while the bottom of the big lobe is centred about −20°, 130°.

Figure A2. Extra figure for the comparison of sampled laboratory experiments of Poch et al. (2016) with the spectra of water-ice-rich features observed on comet 67P and with Hapi region. The spectra are the comparison of ROIs 1–5, 7–10 of Poch et al. (2016) at the beginning of the sublimation experiment with the water-ice-rich features of comet 67P and with Hapi spectra.

Table A1. Coordinates of the features given in Fig. A1. Longitudes are in 0°–360°, latitudes are in ±90 domains.

ID	Longitude (°)	Latitude (°)	Type	Approximate area (m^2)	Early prediction of water ice via multispectral analysis	Water ice reference
1	111	13 N	Cluster	646	–	–
2	117	13 N	Cluster	8373.8	–	Filacchione et al. (2016c, BAP1)
2E	117	13 N	Cluster	77.9	–	–
2W	117	13 N	Cluster	28.1	–	–
3	125	23 N	Isolated	14.4	–	–
4	180	2 S	Cluster	14652.8	Oklay et al. (2016)	Filacchione et al. (2016c, BAP2)
5	182	8 S	Cluster	4652.2	Oklay et al. (2016)	–
6	183	7 S	Isolated	304.0	–	–
7	176	7 S	Isolated	64.0	–	–
8	174	5 S	Isolated	87.7	–	–
9	175	2 S	Isolated	39.27	–	Barucci et al. (2016, spot8)
10	179	1 S	Isolated	395.5	–	–
11	177	5 S	Isolated	368.0	–	–
12E	183	21 S	Isolated	74.5	Oklay et al. (2016)	
12W	183	21 S	Isolated	126.5	Oklay et al. (2016)	Barucci et al. (2016, spot5)
13	183	24 S	Isolated	43.2	–	–
14	189	8 S	Cluster	100.3	–	Barucci et al. (2016, spot7[a])
15	188	8 N	Isolated	73.6	–	–
16	200	12 N	Cluster	1859.2	–	–

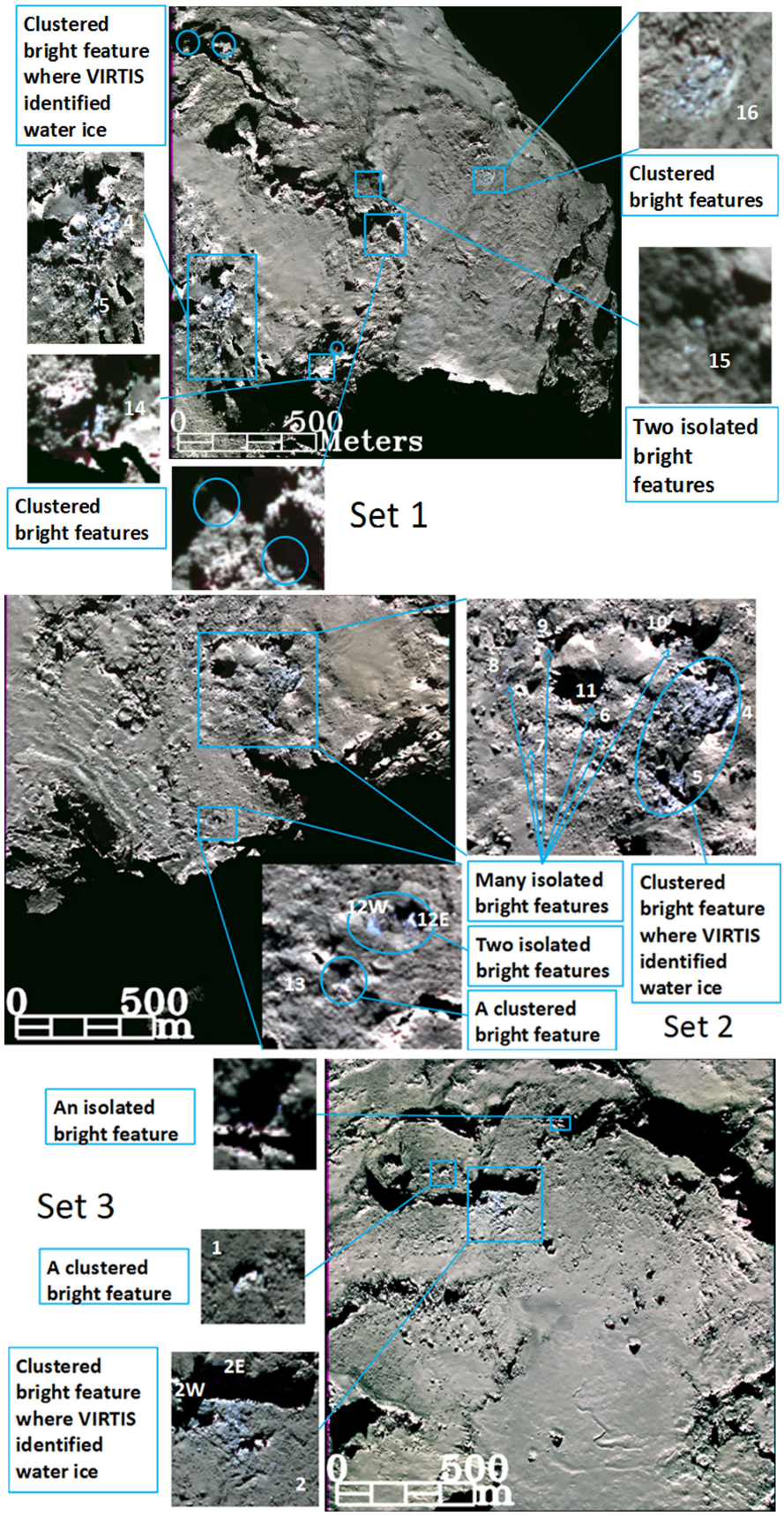[a]In one spot within this cluster, water ice was detected.

APPENDIX B: WATER-ICE-RICH FEATURES ON THE SURFACE OF COMETS

Water-ice-rich features detected on the surface of comet 67P in the investigated images are displayed in Fig. B1. NAC image sets (Table 1) #1–#3 are given from top panel to the bottom, respectively. These features are blue in the RGB composites generated by assigning images taken in 989.3, 649.2 and 360.0 nm to the RGB channels, respectively.
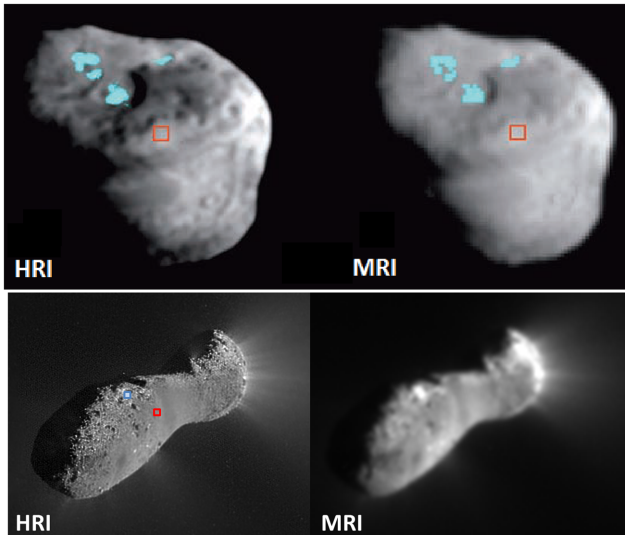
Water ice deposits observed on comets 9P and 103P are given in the top and bottom panels of Fig. B2, respectively. Blue patches indicate the selected ROIs where the mean spectra were calculated. The red rectangles represent the mean surface where the water ice deposit spectra were normalized. The mean spectra of the water ice deposits and the selected surface are normalized at 550 nm for *DI*-HRI data and at 536.0 nm for *DI*-MRI data and presented in Fig. B4 to show the multispectral differences explained in the main text.
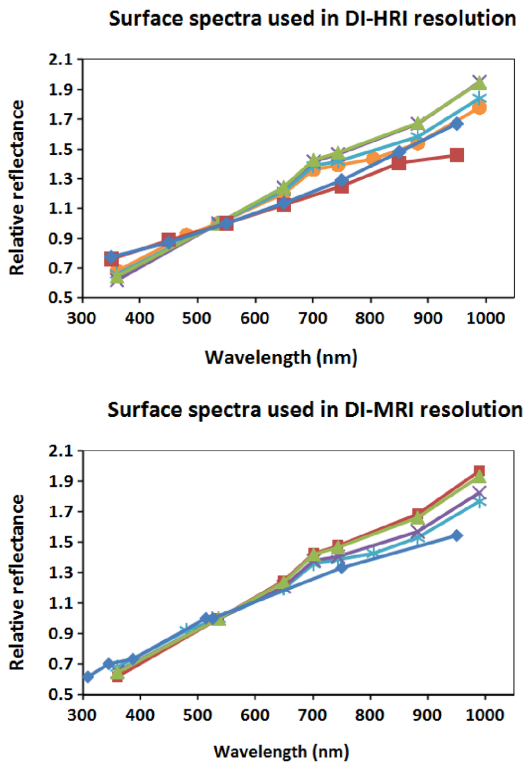
Fig. B3 shows all the mean surface spectra used in the generation of right-hand panels of Figs 4, 5 and 7.
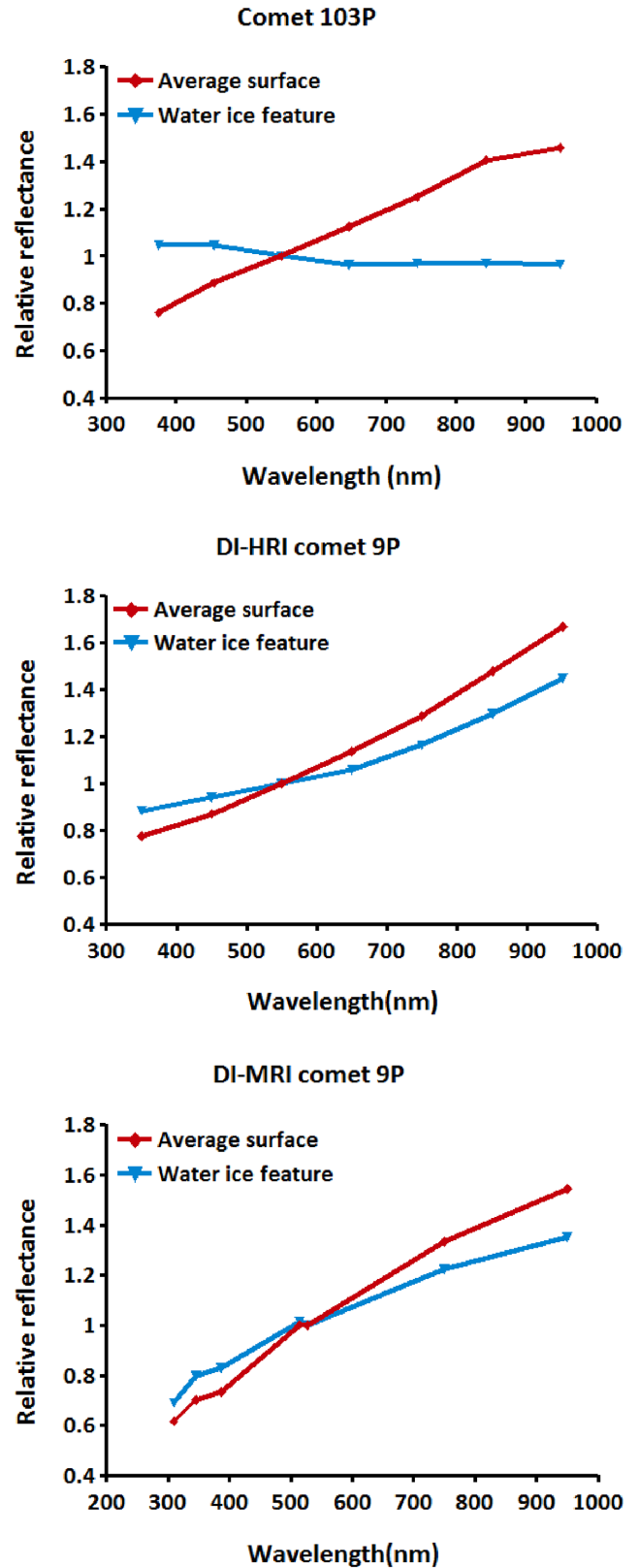
Figure B1. Water-ice-rich and potentially water-ice-rich features seen on the NAC images given in Table 1. The coordinates and approximate size of the features are given in Table A1. The locations of the features are marked in Fig. A1 with the same enumeration.

Figure B2. Water ice deposits observed on comet 9P (top panel) and on comet 103P (bottom panel). Blue patches are the water ice deposits, while red rectangles represent the mean surface.

Figure B3. Mean surface spectra considered in this study. Top panel shows the mean surface spectra used in the right-hand column of Fig. 4 and in the top panel of Fig. 7, while the bottom panel shows the mean surface spectra used in the right-hand column of Fig. 5 and in the bottom panel of Fig. 4.

Figure B4. Mean spectra of the water ice deposits (blue patches) seen in Fig. B2 together with the selected mean surface (red rectangles in Fig. B2). Top panel is the relative reflectance of the water ice deposit observed on comet 103P, while middle and bottom panels show the relative reflectance of the water ice deposits observed on comet 9P in *DI*-HRI and *DI*-MRI resolutions with the average surface spectra, respectively.

APPENDIX C: SAMPLED LABORATORY DATA

Poch et al. (2016) investigated various water ice mixtures in 12 ROI over 40–50 h. In this study, we present only the laboratory spectra which are comparable to the spectra of water ice features observed on comet 67P.

Comparison of ROIs 1–5, 7–10 with the spectra of water-ice-rich features of comet 67P and its Hapi region are presented in Fig. A2 at the beginning of the sublimation experiment.

[1]*Max-Planck-Institut für Sonnensystemforschung, Justus-von-Liebig-Weg 3, D-37077 Göttingen, Germany*

[2]*Department for Astronomy, University of Maryland, College Park, MD 20742-2421, USA*

[3]*NASA Ames Research Center, Moffett Field, CA 94035, USA*

[4]*Center of Studies and Activities for Space, CISAS, 'G. Colombo', University of Padova, Via Venezia 15, I-35131 Padova, Italy*

[5]*Physikalisches Institut, Sidlerstrasse 5, University of Bern, CH-3012 Bern, Switzerland*

[6]*German Aerospace Center (DLR), Institute of Planetary Research, D-12489 Berlin-Adlershof, Germany*

[7]*LESIA, Observatoire de Paris, CNRS, UPMC Univ. Paris 06, 5 Place J. Janssen, F-92195 Meudon Principal Cedex, France*

[8]*Instituto de Astrofisica de Andalucia-CSIC, Glorieta de la Astronomia, E-18008 Granada, Spain*

[9]*Dipartimento di Fisica e Astronomia 'Galileo Galilei', University of Padova, vic. Osservatorio 3, I-35122 Padova, Italy*

[10]*Laboratoire d'Astrophysique de Marseille, UMR 7326 CNRS and Aix-Marseille Université, 38 rue Frédéric Joliot-Curie, F-13388 Marseille cedex 13, France.*

[11]*Centro de Astrobiologia (INTA-CSIC), European Space Agency (ESA), European Space Astronomy Centre (ESAC), PO Box 78, E-28691 Villanueva de la Canada, Madrid, Spain*

[12]*International Space Science Institute, Hallerstrasse 6, CH-3012 Bern, Switzerland*

[13]*Research and Scientific Support Department, European Space Agency, NL-2201 Noordwijk, the Netherlands*

[14]*Department of Physics and Astronomy, Uppsala University, Box 516 SE-75120 Uppsala, Sweden*

[15]*PAS Space Research Center, Bartycka 18A, PL-00716 Warszawa, Poland*

[16]*LATMOS, CNRS/UVSQ/IPSL, 11 Boulevard d'Alembert, F-78280 Guyancourt, France*

[17]*INAF Osservatorio Astronomico di Padova, Vicolo dell'Osservatorio 5, I-35122 Padova, Italy*

[18]*CNR-IFN UOS Padova LUXOR, via Trasea 7, I-35131 Padova, Italy*

[19]*NASA Jet Propulsion Laboratory, 4800 Oak Grove Drive, Pasadena, CA 91109, USA*

[20]*Department of Industrial Engineering University of Padova Via Venezia, 1, I-35131 Padova, Italy*

[21]*University of Trento, via Sommarive, 9, I-38123 Trento, Italy*

[22]*INAF – Osservatorio Astronomico di Trieste, via Tiepolo 11, I-34143 Trieste, Italy*

[23]*Aix Marseille Université, CNRS, LAM (Laboratoire d'Astro-physique de Marseille) UMR 7326, F-13388 Marseille, France*

[24]*Institute for Space Science, National Central University, 32054 Chung-Li, Taiwan*

[25]*Institute for Geophysics and Extraterrestrial Physics, TU Braunschweig, D-38106 Braunschweig, Germany*

[26]*ESA/ESAC, PO Box 78, E-28691 Villanueva de la Cañada, Spain*

[27]*Department of Information Engineering, University of Padova, via Gradenigo 6/B, I-35131 Padova, Italy*

This paper has been typeset from a TeX/LaTeX file prepared by the author.